Femtosecond Laser Interaction with Graphene Oxide Aqueous Solution

Khaled Ibrahim

A thesis

presented to the University of Waterloo

in fulfilment of the

thesis requirement for the degree of

Master of Applied Science

in

Mechanical Engineering

Waterloo, Ontario, Canada, 2015

Author's Declaration

I hereby declare that I am the sole author of this thesis. This is a true copy of the thesis, including any required final revisions, as accepted by my examiners.

I understand that my thesis may be made electronically available to the public.

Abstract

In this study fs pulsed laser of wavelength 800 nm was used to reduce two sets of aqueous graphene oxide solution namely low (0.5 mg/mL) and high concentration (6.2 mg/mL). It was found that after fs laser treatment the surface roughness of the graphene oxide flakes was reduced by 95.6% and 66% for the high and low GO concentration films respectively. It was also found that the resistivity of high concentration (6.2 mg/ml) rGO films was enhanced by 4 orders of magnitude as a result of the laser treatment which could raise the electron mobility of the rGO films close to that of pristine graphene films. The C-O atomic ratio for the high concentration graphene oxide samples was found to increase by 3 times after 6 hrs of laser treatment.

A novel technique of graphene oxide sol-gel (GOSG) fabrication was introduced where GOSG was obtained by placing the laser focal point at the solution/air interface. By manipulating the exposure parameters such as the ablated volume, laser energy and focal length, the GOSG was obtained at various times in the range of as 8 min to 7 hrs. The chemical analysis (XPS) revealed the reduction of the COOH molecules as a result of the exposure process, which is due to removing the OH^- from the GO sheets and vaporization of the water content within the solution. Surface morphology analysis using AFM and SEM showed that all GOSG thin films except the 7 hrs one depicted a high surface roughness and porous surface area with randomly stacked graphene oxide layers. However, a smooth stacking layered structure and the smallest average surface roughness was observed in the 7 hrs GOSG, which was pertained the behaviour of pure graphene as proved by the FTIR analysis.

Acknowledgements

Dedication

To the strongest woman I have ever met, and my best friend. My mother Lolwa Farag.

Table of Contents

List of Figures

List of Tables

List of Abbreviations

Fs	Femtosecond
GO	Graphene oxide
GOSG	Graphene oxide sol-gel
CVD	Chemical vapor deposition
rGO	reduced Graphene oxide
XPS	X-ray photoemission spectroscopy
XRD	X-ray Diffraction
AFM	Atomic Force Microscopy
SEM	Scanning electron microscope
UV VIS	UV visible
FTIR	Fourier Transform Infrared
GOG	Graphene oxide gel
ODA	Octadecylamine
FWHM	Full width half maximum

Chapter 1

Introduction

_____

1.1 Graphene

        1.1.1 Methods of fabrications and applications

        1.1.2 Graphene properties

1.2 Graphene Oxide

        1.2.1 Background

        1.2.2 Synthesis and applications

        1.2.3 Reduced Graphene oxide

        1.2.3.1 Graphene oxide sol-gel

1.3 Thesis overview and motivation

_____

1.1 Graphene

1.1.1 Methods of fabrication and applications

Graphene is a single-layer 2-dimensional, one atom thick (~ 0.345 nm), material consisting of honeycomb lattice of sp^2 bonded carbon atoms [1]. It is one form of carbon allotropes (Fig.1-1) such as charcoal, graphite, and fullerenes. Since Novoselov's et al. success in isolating mono-layered graphene from graphite flakes in 2004 [2], graphene has been subject to intense research by researchers and material scientists. Novoselov's colleague Geim defined graphene "isolated or free-standing graphene" as "graphene is a single atomic plane of graphite [3], which is sufficiently isolated from its environment to be considered free-standing". Graphene has exhibited unique and novel physiochemical properties namely; high fracture toughness, thermal conductivity, Young's modulus and electrical conductivity [2, 4-6]. These remarkable properties consequently enable graphene to possess extraordinary properties such as high mechanical strength and high electrical conductivity. Hence, graphene nano-sheets adapted and settled rapidly in a diversity of applications including energy storage materials, nano-devices, renewable energy development, polymer composites and sensing applications [7-9].
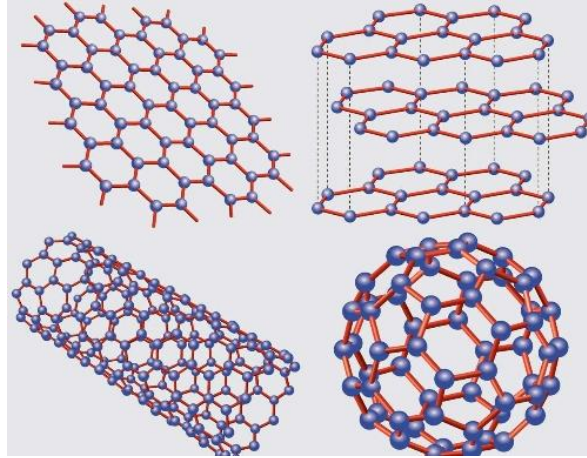
Figure 1-6: Schematic of graphene structure (top left), graphite (top right), carbon nano-tubes (bottom left), and bucky balls (bottom right). Blue balls representing carbon atoms, red connections representing covalent bond [10].

Many researchers have been trying to establish methods of graphene fabrication on a large scale dated back to 2004, thus attempts such as epitaxial growth on non-metallic substrates [11] and chemical vapor deposition techniques [12] have been established. There are many ways for single layer and multilayer graphene fabrication such as micro mechanical cleavage, CVD on metallic substrate, intercalation of graphite and graphene oxide single layer reduction, comprise chemical reduction of exfoliated graphene oxide, arc discharge and thermal exfoliation of graphite oxide [13].

Graphene sheets can be fabricated via the scotch tape method, which yields flat stacked graphene sheets as a result of cleavage of graphite [2]. Due to graphene sheets high specific area (atomic density per unit area), it sometimes tends to re-stack and form irreversible bulk graphite as a result of van der Waals interaction between the graphene sheets [14]. Graphene has been prepared using chemical processes such as graphite oxidation, chemical exfoliation and reduction, given its low cost and large scale fabrication ability [15].

1.1.2 Graphene Properties

Due to its extraordinary electrical and mechanical properties such as large surface-to-volume ratio [16], superior optical properties [1], large carrier mobility (surpassing 20000 cm^2 V^{-1} s^{-1}) [17], high thermal conductivity, high mechanical strength (e.g. 200 times greater than steel) and tensile modulus of 1 TPa [18], graphene becomes a material of great interest to optoelectronic, MEMS and NEMS applications. Excellent electrical conductivity is key for conduction of the biomolecules for sensing applications, given its extremely high electron speed propagation attributed to the absence of a band gap. Carbon has 6 electrons with 2 electrons in the inner shell, and 4 electrons on the outer shell. In a typical situation, an individual carbon atom usually offers its four electrons of the outer shell for bonding. On the contrary, carbon atoms in graphene are connected to three other carbon atoms on a 2-dimensional plane in a very strong covalent bond also known as the sigma bond, hence leaving a lone electron on the third dimension performing an electronic conduction role. This freely available electron are called π electrons that are located on z-axis, thus orbiting above and below the graphene sheet as schematically shown in Fig.1-2.

The π electrons consequently overlap with neighbouring lone electrons on the sample plane forming the pi-bond. Effectively, the bonding and anti-bonding of these lone electrons dictate the electronic properties of graphene.
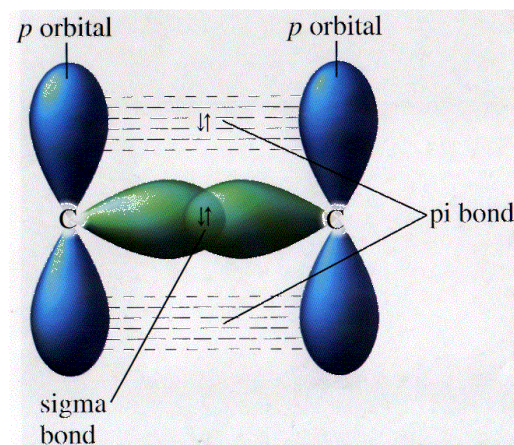
Figure 1-2: Schematic of sigma and the overlapping pi bonding of carbon atoms [19]

1.2 Graphene oxide

1.2.1 Background

Graphene can be fabricated in many different ways such as epitaxial growth and chemical vapour deposition as previously mentioned. However reducing oxygen functional groups in graphene oxide is one of the most reliable methods of graphene fabrication in the research labs.

Most importantly, graphite oxide becomes hydrophilic. Being hydrophilic enables the graphite oxide to be exfoliated into single or few layers of graphene oxide by means of sonification. Graphite oxide differs from graphene oxide in the number of layers. While graphite oxide is known to attain to multilayer system, graphene oxide is usual to find few layered flakes and single layered graphene oxide.

1.2.2 Graphene oxide fabrication and its applications

Graphene oxide can be fabricated in a variety of techniques, which are usually hazardous, lengthy in time and inefficient. In 1958, Hummers-Watson method was introduced to produce graphene oxide as a safer, faster and more efficient way [20]. After slight modifications [21], Hummers method becomes the most widely used technique amongst researchers and material scientists to produce graphite oxide due to its ease, simplicity and short time process. Hummer-Watson method includes the harsh induction of strong chemical solvents such as sulphuric acid, potassium permanganate and sodium nitrate to the graphite to oxidize graphite-to-graphite oxide before sonification in aqueous solutions to fabricate graphene oxide. Several modifications and improvements were studied by removing the sodium nitrate from the oxidation process [21].

Graphene oxide is used in a myriad of applications, most notably; as a building block in nano-devices such as transistors and sensors. Graphene oxide performs the role of the semi-conductor, with the oxygen functional groups inducing a band gap enabling the graphene oxide to act as an insulator and control the switch of the respective device.

1.2.3 Reduced graphene oxide

Significant effort was focused on developing the methods to successfully fabricate and reduce graphene oxide, researchers are competing in innovating and developing these methods aiming to produce the highest quality of graphene whether it be in solution or in solid state. Comprehending the reduction process of graphene is invaluable for further improvements and exploitations of reduced graphene oxide processes on an industrial scale. Over the years, reduction techniques introduced varied depending on the several chemical reactions such as using sodium borohydride, hydrazine-assisted reduction of graphene oxide, catalytic, plasma induced, thermal and hydrothermal reduction techniques were all achieved proper level of reduced graphene oxide. Although each method has its own merits and drawbacks, photo-assisted reduction promises to be one of the most facile, dependable and rapid ways to reduce graphene oxide successfully without usage of harsh and toxic chemicals. Several laser wavelength's and pulse intensities were used on GO solution to yield rGO of different properties in various times. In this study fs laser pulses were used to reduce the oxygen functional groups in graphene oxide flakes, where the effect of using this method in terms of characterization and methodology is going to be thoroughly discussed and analyzed.

1.2.3.1 Graphene oxide gel

Previous studies discussed paper-like materials, thin film and freestanding films of graphene oxide. In comparison to 2-dimensional monolayers, 3-dimensional graphene based material display various advantages including high surface area and a myriad of physical and electronic properties stemming from their different morphology [22]. Graphene 3D gel and sol-gel is used in several applications such as catalysis, drug delivery, energy storage improvement, sensors and actuators [7, 23-25]. To fit in such applications, the main challenge is assembling these graphene sheets structures into a gel/sol-gel like texture, with controllable pore size and inter-layer distance [26]. It has been reported that these graphene gel-like structures were formed through π-π interactions between the graphene sheets offering a linker

such as divalent ions after using the hydrothermal process [27]. Graphene oxide gel structures have been a recent revelation in terms of the synthesis techniques using the addition of hydrophilic polymers or metallic ion cross-linkers to trigger the electrostatic interaction between the graphene sheets. In this study, a novel technique of graphene oxide sol-gel formation is previewed and is studied.

1.3 Thesis overview and motivation

This study focuses on the reduction techniques using fs pulsed laser to reduce graphene oxide. Graphene oxide reduction methods such as chemical reduction, and irradiation techniques will all be discussed in detail in Chapter 2. This work will discuss fs laser interaction with both low (0.5 g/L) and high (6.2 g/L) concentration graphene oxide. Graphene oxide sol-gel was obtained in a novel fabrication technique, where the graphene oxide solution was exposed by placing the laser focal point at the surface rather than placing the focal point inside the solution. The location of the laser focal point affected the yielded material to be sol-gel. A series of laser energies and solution volumes were employed to obtain the graphene oxide sol-gel (GOSG) in various times.

The fabrication method of reduced graphene oxide solution samples (low concentration, high concentration, and GOSG) using the fs laser are discussed in Chapter 3. Different characterization tools were employed to examine and investigate the rGO and GOSG properties, such as electrical, surface morphology, and chemical properties, which is also discussed in Chapter 3. The results and discussion of the obtained experimental data are analyzed thoroughly in Chapters 4 and 5.

Chapter 2

Graphene Oxide Reduction

_____

2.1 Introduction

2.2 Graphene oxide reduction techniques

        2.2.1 Graphene oxide reduction via photo-irradiation techniques

        2.2.2 Chemical reduction of graphene oxide

2.3 Graphene oxide sol-gel

2.4 Summary

_____

2.1 Introduction

This chapter focuses on some of the previous works that have been implemented in the aims of reducing graphene oxide using several methods and techniques. In section 2.2, the various methods in which reduction of the graphene oxide from its oxygen functional groups will be studied. Chemical solvents are a common additive to graphene oxide enabling a reduction process of the graphene oxide, and also refining the graphene oxide flake and features. However, Photo-irradiation is an alternative way of reducing the graphene oxide aqueous solution.

The graphene oxide sol-gel will also be studied with regards to recent works and development and are discussed in section 2.3.

2.2 Reduced graphene oxide techniques

Production of a high quality graphene flake/sheet has recently been an area of intense research by numerous material scientists and researchers in academic institutions. This can be done in a cost-effective manner by reducing the graphene oxide to obtain reduced graphene oxide (rGO). The setback with reducing GO is that some methods yield graphene sheets of a quality in close vicinity of pristine graphene. In other words, the level of defects within the graphene sheets yielded by some of these

techniques does not match the potential of pristine graphene in comparison to other techniques such as mechanical exfoliation.

The method in which graphene oxide reduction is carried out determines the defect ratio of the graphene flakes hence its quality [28]. When large scale processes is a necessity and a large quantity of graphene is required such as in industrial applications (i.e. energy storage), rGO is utilized frequently [29] due to the fact that it is relatively easy to fabricate and therefore the graphene quality is crucial.

As mentioned there are numerous methods in which graphene oxide can be reduced, namely chemical, thermal, photo-irradiation, and electro-chemical techniques. Although some of these methods yield high quality graphene oxide pertaining to the coveted characteristics of pristine graphene, some techniques tend to be lengthy and complicated processes to accomplish.

2.2.1 Graphene oxide reduction via photo-irradiation techniques

Different photo-irradiation techniques have been used to expose graphene oxide aiming to complete a reduction process. Laser irradiation reduction has been a common method to successfully reduce graphene oxide, different pulsed laser such as nano, pico and fs lasers have been subject to research in terms of their interaction with graphene oxide [30-32]. This technique depends on focusing a huge energy on the graphene oxide and causing ionization thus reducing the oxygen functional groups from the graphene oxide networks. This technique is generally favored rather than other techniques given it is a facile and rapid technique [33].

Han Wei Chang et al. investigated the reduction of graphene oxide by means of fs laser irradiation [32]. 4 mL of the GO solution was exposed by fs laser with pulse intensity of 1.5×10^{15} W/cm^2 and operating wavelength of 800 nm. The laser focal point was irradiated perpendicularly inside the solution, whilst it was focused using an aspheric lens with an 8mm focal lens and a 0.5 numerical aperture. The laser was irradiated for different intervals of time (0, 1, 5, 10, 20, 30 and 60 minutes) to study how the solution behaved throughout the span of the irradiation process.

8
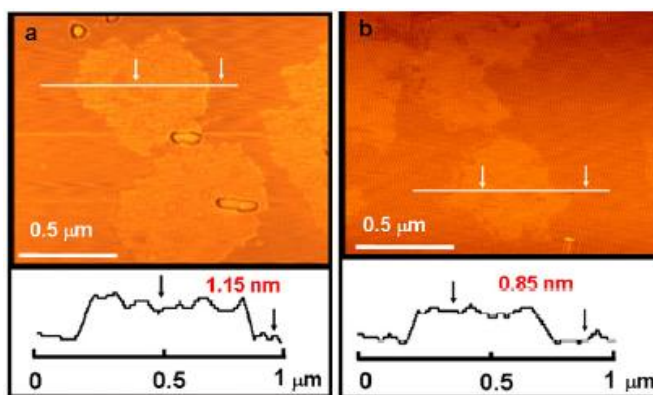
Figure 2-1: The AFM images of (a) Graphene oxide and (b) reduced graphene oxide flake [32]

The XPS analysis showed a significant reduction of the C-O peak with the increased laser exposure time. It was also found that the atomic carbon-to-oxygen ratio was increased from 1.7 to 8.1 (GO to rGO respectively), an analytical indication to the successful reduction of graphene oxide. The AFM images (Fig.2-1) also shows the reduction of the thickness of the graphene oxide flakes. The flake thickness of a given flake in the rGO was measured as 0.85 nm whilst the GO flake was measured as 1.15 nm. This reduction in thickness was attributed to the loss of oxygen groups. The UV-VIS spectroscopy showed a redshift of π-π^* transition from 233 nm (GO solution) to 262 nm (rGO solution) followed by increase in the absorption which confirmed the reduction of oxygen functional groups in the graphene oxide.

Laser assisted graphene oxide reduction was also reported by Lei Huang et. al. [34]. 15mL of the GO solution were loaded in a quartz tube with magnetic stirrer. The laser utilized in irradiating the solution had a repetition rate of 5 kHz, laser energy of 200 mJ, focal length 30cm, pulse width of 20 nm, wavelength of 248nm and exposure was carried out for 5 minutes. The magnetic stirrer was employed to keep stirring the solution within the quartz tube throughout the whole procedure to ensure that the exposed areas were homogenous at all times of exposure.

The XRD analysis of graphite showed the (002) plane peak at 26.60^o while the as prepared GO showed a (001) peak that was recorded at 11.38^o. It was found that the (001) peak intensity in the rGO was reduced gradually by increasing the exposure time. This is a clear indication that the GO reduction was successful, however; the rGO sheets were yet greatly disordered [35]. The UV-VIS spectroscopy has shown an increase in the absorbance of the GO with ammonia in comparison to the as-prepared GO as it is clear from Fig.2-2a-c. The reduction process that was completed by the laser has partially removed a percentage of the oxygen functional groups and hence the formation of rGO was attributed to strengthened electrostatic stabilization with ammonia. The electrical conjugation was restored as shown in absorbance increases with increasing of the exposure time from 10s to 5min.

The calculated I_D/I_G ratio were reported as 1.03 and 1.08 for the GO and the rGO respectively, showing slight decrease in the sp^2 clusters size from 4.3 nm to 4.1 nm. Fig.2-2a shows the SEM images of thin folding of the as-prepared GO structure, whilst on the irradiated rGO (Fig.2-2b) thick crumpled structure of aggregated flakes were observed. Although the AFM images indicated a similar flake thickness for both as-prepared and irradiated rGO, it was found that the irradiated flakes were dispersed and separated contrary to the aggregation of the as prepared GO.
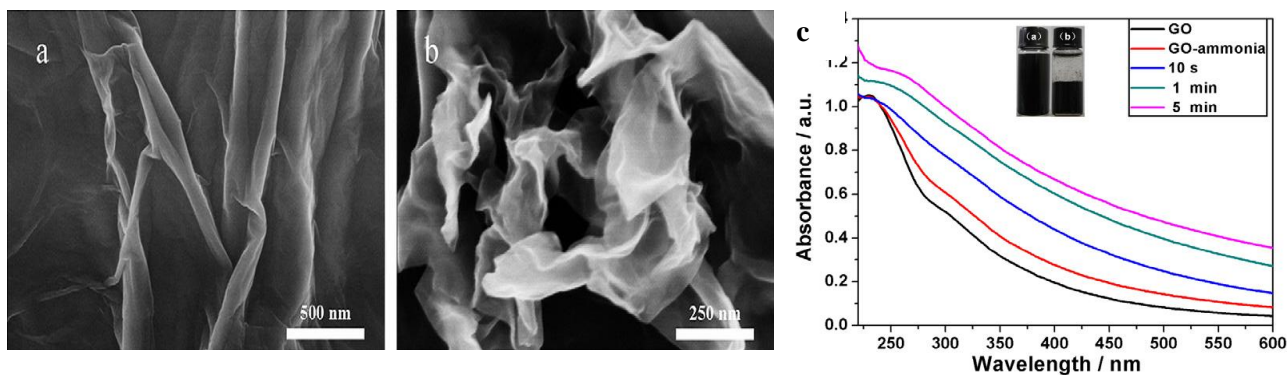
Figure 2-2: UV visible spectrums obtained as a result of laser irradiation and mixing GO with ammonia. SEM images for (a) as-prepared GO and (b) Irradiated rGO [34].

Regis Y.N. Gengler et al. reported a method where graphene oxide is reduced utilizing ultraviolet fs pulsed laser in a photo-reduction phenomena [36]. The process was done in a pump-probe fashion were a steady flow of suspended GO streams and was irradiated via ultraviolet fs pulse performing the role of the pump, directly followed by another visible fs laser pulse irradiation performing the role of the probe. UV-VIS spectroscopy was carried out on both unexposed and irradiated sample to confirm the identity of the photoproduct. It was found that the rGO offered a higher absorbance levels over the span of the absorption range (i.e. 280 nm to 800 nm) which confirmed the restoration of the π networks within the carbon structures. The XPS spectrum (Fig.2-3) confirmed the process successfulness by illustrating a dramatic drop in the C–O, C=O, C–O–C and C(O)O peaks, accompanied with increases of the C-C bond from 8 % to 66 %.
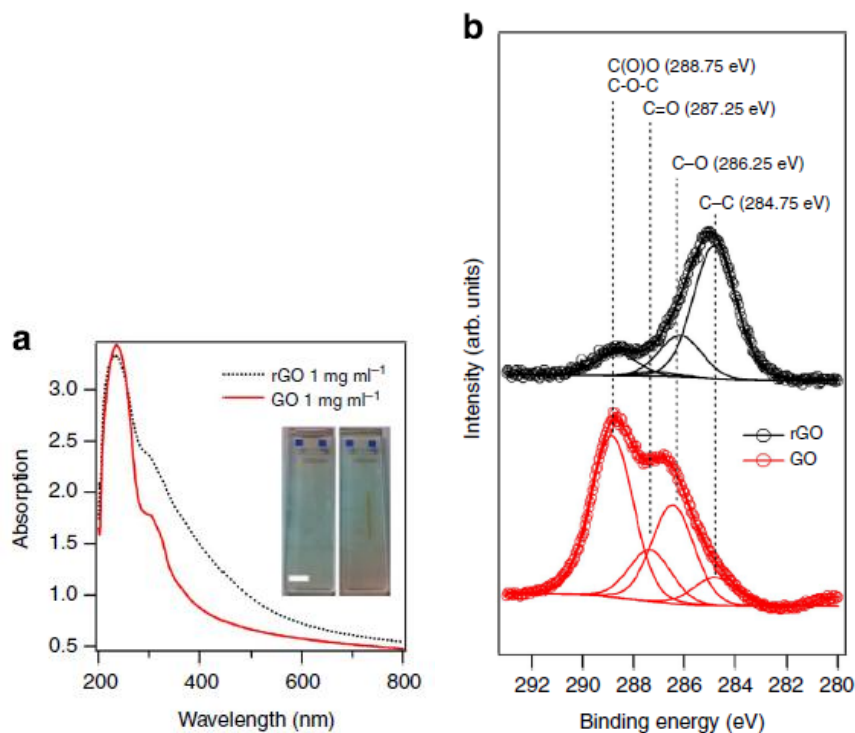
Figure 2-3 : (a) The UV-VIS spectrum of GO and rGO and (b) XPS spectrum for the GO and rGO [36].

11

In-situ reduction of graphene oxide solid films was an alternative way to reduce the oxygen functional groups from graphene oxide film. Emmanuel Kymakis et al.[37] have studied the effect of fs pulse irradiation with graphene oxide deposited on thick substrate polyethylene terephthalate (PET) by using spin coating technique, the exposure process involves a large surface area (15x15 mm) as reported.

A Ti:Sapphire laser with a 10 mm focal lens, operating wavelength of 800 nm, repetition rate of 1 kHz, 100 fs pulse width and output power in the ranging of 1.0 mW to 10 mW was utilized to irradiate the GO thin film which was placed on a high precision x-y translation stage perpendicular. A mechanical shutter ensured the uniformity of the exposure with the sample being exposed to a constant number of pulses. A schematic diagram of the exposure setup is shown in Fig.2-4.
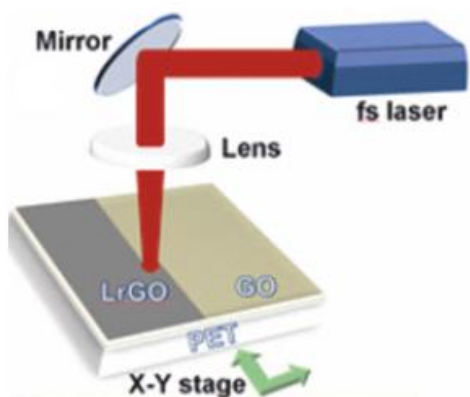
Figure 2-7: Schematic diagram of the exposure setup for the GO film irradiated by fs laser pulse [37].

It was found that the micromachining did not affect the mean surface roughness of the graphene. The beam was translated onto the surface area of the substrate and it was observed that the yellow color of the film started to transform into a black color, which is a preliminary observation of reduction process. The reduction process was also controlled by mean of altering the irradiation power from 3mW to 10mW. Furthermore, by deconvolution of the XPS spectrum, three major peaks were yielded corresponding to C-C (non-oxygenated), C-O, C=O. It was observed that the oxygenated carbon molecules were reduced

from 61 % to 16 % from the GO to the rGO respectively. The significant decreases in oxygen intensity could be attributed to reduction of the oxygen functional groups. It was reported that major improvements could be implemented without incurring any damage on either the graphene or the PET substrate.

Sheet resistance was also measured with respect to two other parameters, namely laser power and number of pulses per spot. Fig.2-5a shows the effect of the exposure power on the sheet resistance; the sheet resistance value was significantly reduced as a result of increasing the laser energy. As can be seen from the figure, the conductivity was increased by two orders of magnitude by increasing the laser power over 5.5 mW. It was reported that the number of pulses per spot (N) have significant effect on the sheet resistance as shown in Fig.2-5b. The resistance was decreased as a result of increasing N until a saturation threshold was reached. It can be concluded that an optimized combination between laser energy and N can yield a massive reduction in the sheet resistance.
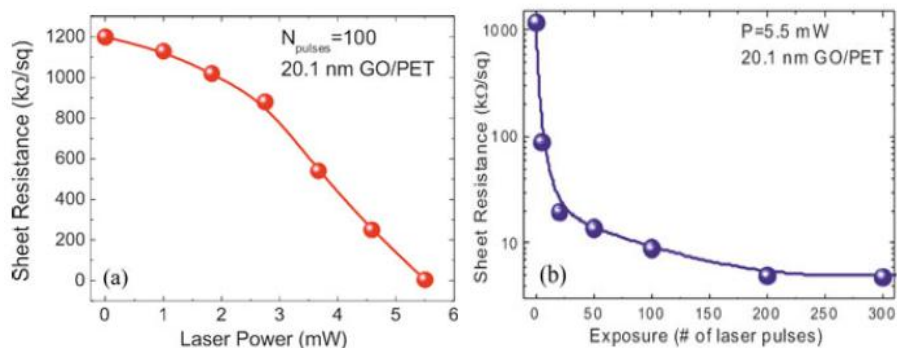
Figure 2-8 : Sheet resistance of the rGO film as a function of (a) the laser power and (b) the number of pulses per spot [37]

Simon Spano et.al. [38] investigated the effect of a different pulse duration laser interaction with graphene oxide. The graphene oxide was exposed to a Continuum Surelite (Nd:YAG) laser (λ= 532 nm, pulse duration 5 ns, repetition rate of 10 Hz, beam diameter of 28 mm^2). The laser beam was focused directly at the solution without employing any focusing lens with power density of 0.32 J/cm^2 at different time in the range of 15 min to 300 min. The gradual blackening of the solution with increasing exposure

time was observed. The absorption spectral analysis showed a distinguishable peak at wavelength of 230nm which corresponds to the transitions within the C=C bond [39] and a shoulder at wavelength of 300 nm attributed to the sp^3 hybridized C=O bonds [39]. It was found that by increasing the exposure time a redshift towards larger wavelength was recorded at wavelength of 230 nm and the shoulder peak at wavelength of 300 nm was disappeared. These effects could be due to the restoration of the carbon networks.

The FTIR spectrum of both GO and partially reduced GO are compared in Fig.2-6a. As can be seen from this figure the main molecular absorption sites were OH stretch (3420 cm^{-1}), C=O carbonyl stretching (1735 cm^{-1}), in-plane vibration C=C (1622 cm^{-1}), epoxy groups (1220 cm^{-1}) and stretching C-O (1110 cm^{-1}) [40-42]. Fig.2-6b shows the FTIR spectrum of partially rGO in the range of 3000 cm^{-1} to 300 cm^{-1}. From this figure, it is clear that a significant reduction of the absorbance was recorded at wavenumber of 1080 cm^{-1} and 890 cm^{-1} which belong to the epoxy groups. The absence of these oxygen rich functional groups and restoration of the sp^2 hybridization of carbon could be due to the laser effect [38].
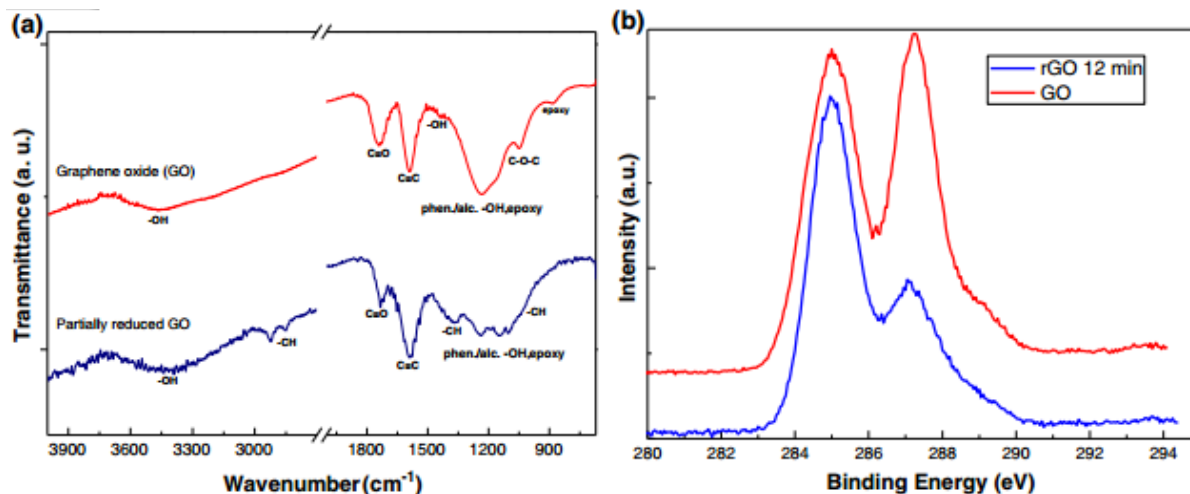
Figure 2-9: The (a) FTIR (b) XPS spectrum of both untreated graphene oxide and partially reduced graphene oxide[38].

Fig.2-6b show the XPS spectrum of both GO and partially rGO. The peaks correspond to C-C, C-O and O-C=O were recorded at 284.5 eV, 287 eV and 289 eV respectively. The peak intensity at 287.3 eV could be attributed to the reduction of the amount of the oxygen functional groups [43].

Reduced graphene oxide could also be acquired by using high power UV light. Tongshun Wu et. al. [44] studied the reduction of graphene oxide using UV light irradiation [44]. An 0.3 mL of homogenized GO solution was mixed with 2.7 mL of dimethylformamide (DMF) which serves as both electron-donor and solvent. The mixed solution was then exposed to a UV mercury lamp, with power of 200 W and working distance of 5 cm between the lamp and the solution for 60 min. The system was covered with a water cooling system. Wu also mentioned that such process can be carried out similarly in a mild fashion by exposing the mixture to sunlight for 3hrs to complete the reduction process [44]. Fig.2-7, shows the
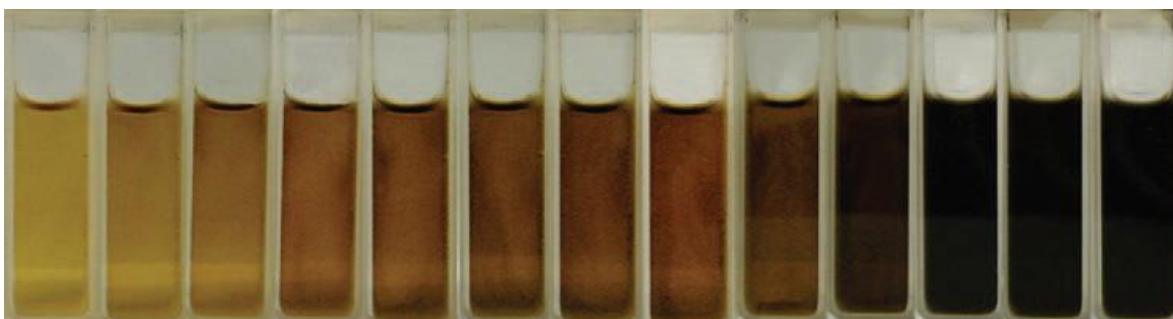
images of the obtained solution every 5 minutes. From this figure it can be seen that the solution turns from pale-yellow to black after 60 min by completing the reduction process.

Figure 2-10: The GO solution color changes from pale-yellow towards black Images are captured every 5min interval [44].

The UV-VIS spectrum shows a redshift in the absorption peak from 238 nm to 273 nm accompanied with a general increase in absorbance intensity by increasing exposure time. Such increase in absorbance intensity was attributed to the restoration of the electronic configuration amongst the graphene networks. The recorded XPS spectrum emphasized the success of reduction by photo catalytic phenomenon. The C-C (characteristic of graphite), C-O and C=O feature were recorded at 284.6 eV, 286.6 eV and 288.5 eV respectively. It was found that the intensity of the oxygen functional group peaks were reduced from 44.2 % to 15.9 % proving the reduction of the sp^3 and sp^2 oxygen bonds within the graphene networks [44].

15

Raman spectroscopy showed the presence of two strong D and G bands at 1350 cm^{-1} and 1575 cm^{-1} respectively. The defect ratio increased from 0.78 to 1.06 indicating the formation of graphitic domains. Guardia et.al. [45] also studied the direct reduction of graphene oxide aqueous solution by means of exposure to UV light. Similar to the previous studies [46, 47] graphene oxide solution was prepared using modified Hummers method [45]. The photo reduction process was carried out by exposing the graphene oxide solution to 50 W UV light generated by a short arc mercury bulb which emits in the range of 280 nm to 450 nm. The aqueous graphene oxide solution was placed at a distance of 15 mm from the UV lamp, and the exposure utilized for different time in the ranged 5 min to 24 hrs. The UV-VIS spectroscopy was performed similar results to previous works [32, 34] for both untreated GO and rGO. The optimized rGO which was treated for 5.5 hrs to the UV light irradiation was shown a 30 nm redshift for absorption peak at wavelength of 230 nm following by disappearing the shoulder peak at wavelength of 300nm. The absence of absorption feature at wavelength of 300 nm could not be due to the reduction of the C=O transition, because the XPS analysis shows (Fig.2-8a) the C=O bond has not been significantly removed and therefore it is not affected by the reduction process [45]. Both the redshift occurring at wavelength of 231 nm and increases of absorbance intensity caused the shoulder to not be as prominent and thus the peak hides as a result.
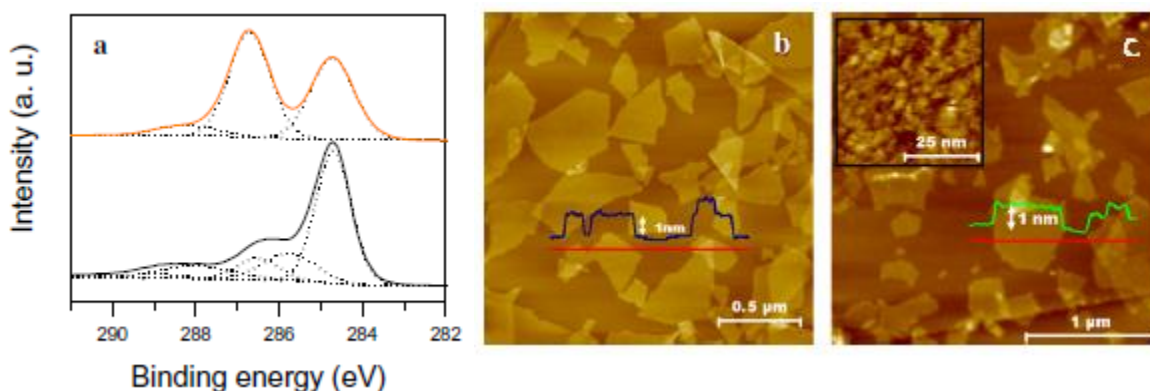
Figure 2-8: (a) The XPS spectrum of both untreated GO dispersion (orange) and UV irradiated GO (black). The AFM images of (b) untreated GO (c) rGO. Inset of (c) shows higher magnification scale[45].

Fig.2-8b shows the graphene oxide flakes of the untreated GO, whereas the lateral dimensions of the flakes range about a few hundred nanometers and thickness of 1 nm. As can be seen from Fig.2-8c, no agglomeration of the flakes were observed in the rGO sample, while high surface roughness were recorded which could be attributed to the distortion of the carbon structure due to the surface defects. Such surface morphology was also observed in the rGO using hydrazination technique [48] to produce reduced graphene oxide [49].

2.2.2 Chemical reduction of graphene oxide

Chemical assisted reduction of GO is one of the main reduction methods utilized to achieve rGO. In this section some previous works that employed chemical solvents/agents to produce rGO solutions are reviewed briefly.

Harshal P. Mangse and co-workers [50] studied the chemical functionalization of graphene oxide hence reducing it successfully [50]. Hydrazine monohydrate was used as the reducing agent to suspend the obtained aqueous dispersion of GO. This mixing process was carried out for 24 hours where the black rGO solution was acquired showing the removal of the oxygen groups and the restoration of the π-conjugated graphene oxide networks during the reduction process.

XPS analysis was carried out to monitor the chemical alterations that happened to the GO as a result of the Octadecylamine (ODA) addition as shown in Fig. 2-12. The C-C, C-O, C-O-C and COOH features were recorded at binding energy of 284.5 eV, 286.5 eV, 288.2 eV and 289.2 eV respectively. The XPS analysis of the 1Cs transition in the GO solution shows that two overlapping peak structures followed by a broad series of peak with lower intensities at larger binding energy, which is an indication of oxygen functional groups being attached to the carbon networks. The rGO-ODA XPS analysis showed one high intensity peak at 287eV followed by a series of low intensity broad peaks. The contribution of ODA caused an increase in the intensity of the C-C bond (284.5 eV) followed by decreases in the intensity of
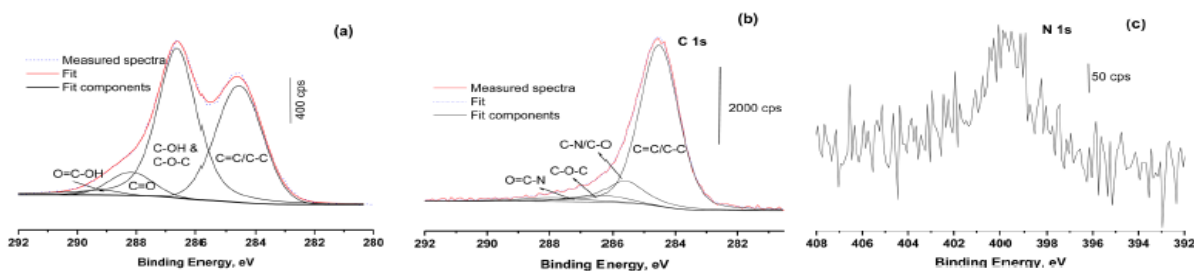
the oxygen containing bonds. The addition of ODA to rGO resulted in the emergence of three new chemical bonds with low intensities at binding energy of 285.6 eV 286.5 eV and 288.0 eV which were assigned to the C-N/C-O, ether group (C-O-C) and amide group CONH-R respectively [51, 52]. The amide group also caused an appearance of a non-intense nitrogen peak.

Figure 2-9: High resolution XPS spectra of (a) untreated GO (b) ODA reduced GO and (c) N1s peak of ODA-rGO [50]

In another work, thiophene was utilized dual function reduction method [53], where the thiophene was added as chemical solvent to the GO for its ability to act as an electron donor and to consume oxygen and performing the reduction process. It is believed that thiophene could act as a mildly reducing agent and thus could be an effective technique to mass produce rGO from GO by oxidation of polythiophene sulfoxide or sulfone through releasing of the electrons and consuming the oxygen. GO was then suspended in 10 mL of deionized water via stirring at room temperature, 2 mL of the thiophene solution were then added to the suspension. The resultant solution was then heated at 80°C for 24 hrs, the solution was then filtered and rinsed using water, ethanol and acetone before being dried at 60°C for another 24 hours to obtain the rGO powder. The XPS analysis of the rGO powders confirmed that the oxygen containg bonds were severley reduced relative to the untreated GO. The carbon-to-oxygen (C-O) atomic ratio of the untreated GO was calculated as 2.0 which shows a large possesion of oxygen groups in the GO powder. Whilst, the C-O atomic ratio of the rGO powders was calculated as 10.9 which indicates the removal of the oxygen functional groups. There were no sulphur related groups in the e XPS spectrum which confirmed that this solvent could successfully be used to reduce the oxygen functional groups in the GO without any contamination.

The Raman spectroscopy of both untrated GO and rGO were caried out and the D and G band were recorded at wavenumber of 1352 cm^{-1} and 1605 cm^{-1} respectively. The defect ratio was calculated as 0.91 and 0.41 for both GO and rGO powders respectively. The significant reduction in defect ratio was attributed to the healing role of the thiophene solvent [54]. Furthermore, increasing thiophene solvent volume to 0.2, 1 and 5 mL resulted in reduction of the defect ratio to 0.81, 0.65 and 0.43 respectively.

2.3 Graphene oxide sol-gel

The fabrication of the 3 dimensional networks of graphene and graphene oxide to form gel medium has gained much attention from researchers around the world due to the wide range of applications such as energy harvesting, biomedical, health care and electrochemistry. Different studies were carried out for graphene oxide gel and graphene oxide sol-gel fabrication [25, 55].

Xu et. al. [27] study the GO gel formation using, 10mL of homogenous GO dispersion with concentration of 2 mg/mL, 0.1 mg/mL, 0.5 mg/mL and 1.0 mg/mL sealed in Teflon-lined autoclave and left for 44 hrs at $180^{o}C$ before cool down to room temperature. The lateral dimension effect of graphene oxide investigated using sonicator bath for 1 hr.
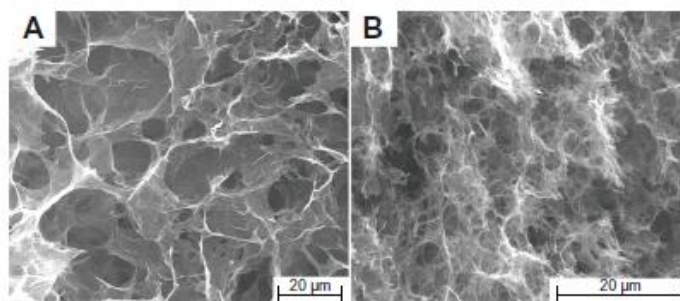
Figure 2-10: The SEM images of (a) 2 mg/ml GO gel and (b) 1 hr sonicated GO gel [27, 55].

Fig.2-10 shows, the SEM images of GO gel and sonicated GO gel with GO concnetration of 2 mg/ml. It was found that both structures offered defined, interlinked graphene oxide structure. The pores observed suggested a sponge-like structure. Unlike to GO gel, the sonicated GO gel was shown smaller pore size as a result of the smaller graphene sheet size achieved from the shattering of the sonification.

19

XRD spectrum of graphene hydrogels is shown in Fig.2-11. As can be seen from this figure the diffraction peaks were recorded at 26.5°, 9.1° for pristine graphite and GO respectively. There were no significant changes in the recorded XRD peaks in the GO gel by increasing the GO concentration from 0.5mg/ml (θ=13.5) to 2 mg/ml (θ=13.7). The interlayer distance of the GO and GO gels were calculated as 3.36 A°, 9.68 A°, 6.55 A°, and 6.45 A° respectively for pristine graphite, GO, GO gel (0.5 mg/ml) and GO gel with GO concentration of 2 mg/ml. The XRD analysis showed that the interlayer distance for the pristine graphite reduced compare to that one in graphene oxide due to the absence of oxygen functional groups within the pristine graphene. The hydrothermal process applied on the GO gel formation resulted in the smaller interlayer distance than that of GO, which could be due to the removal of oxygen functional groups such as -OH groups where can be verified by FTIR spectroscopy.
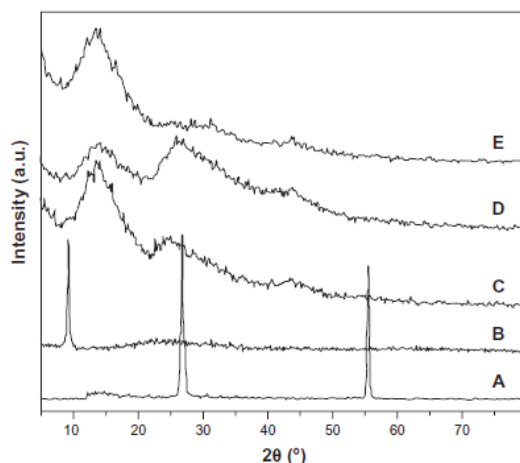
Figure 2-11: The recorded XRD spectrum of (a) pristine graphene, (b) graphene oxide nanosheets, (c) GO gel with GO concentration of 0.5mg/ml, (d) GO gel with GO concentration of 2 mg/ml and (e)sonicated GO gel with GO concentration of 2mg/ml [27].

The GO gel could also be fabricated using supermolecular self-assembly [56]. The GO was added to a mixture of deionized water and ethanol (DI: ethanol=1:1) followed by 1 hr sonication. Furthermore, 5 mL of Ferocene (FC) was added to the mixture and shaken well and the solution was kept to rest for 30 min where yielded to the graphene oxide gel (GOG). Ethanol was easily removed by water exchange and freeze-drying process. The FC played a crucial role in the formation of 3D structures of graphene oxide gel and interlayer cross linker by means of the π-π interaction [57].
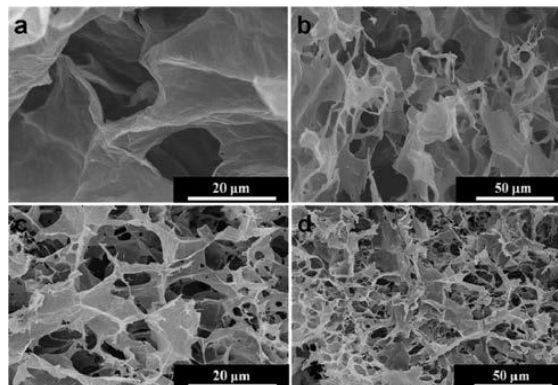
Figure 2-12: The SEM images of (a) freeze dried GO (b) GO gel fabricated using supermolecular self-assembly technique [56].

Fig.2-12a and Fig.2-1b shows the SEM images of the freeze dried GO and GO gel. The freeze dried GO offered a large disorder and porous networks which was attributed to the aggregated graphene oxide sheets [55]. While Fig.2-12c and Fig.2-12d show that GOG presents an interconnected 3D porous network assembly of GOS.

2.4 Summary

This chapter discussed previous research on graphene oxide oxygen functionl group reduction techniques and methodologies, such as photo-irradiation, chemical assisted reduction and formation of graphene oxide gel/ sol-gel as a result of reduction. Chemical assisted reduction methods, also frequently involved thermal treatment of the GO solution, whereas the added chemical solvents were found to intake the functionalities of oxygen, before rinsing and washing of the reduced graphene oxide to obtain rGO. However, these chemical reduction techniques have intrinsic disadvantages, for instance; the usage of toxic chemical solvents such as hydrazine, requirement of high acidity levels, high thermal treatment, and need of special instruments restrict the wide range synthesis of rGO. The photo-irradiation techniques depend on using high energitic photons, hence ablating the graphene oxide and interacting with molecules to remove the oxygen functional groups.

However, it was clear that photon-irradiation techniques used to reduce graphene oxide were done in significantly shorter processing time, some methods included thermal treatement for prolonged times ranging from 20 hrs to 44 hrs. Therefore, photo-irradiation based reduction specfically pulsed laser irradiation of graphene oxide was found to be completed in a short processing time as low as few minutes. Consequently, a wide range of quality and purity rGO soultions and films could be achieved. Although most of the chemical assisted reduction procedures resulted in smooth and thin GO layer, each technique consists of its drawback and advantages, paving the way for a diversity of applications for the GO to be employed in.

Chapter 3

Experimental Methodology and Spectroscopy

_____

_____

3.1 Introduction

This chapter will review a description of the experimental procedures using various equipment, machines, tools and techniques on course towards completing this research. In this chapter, the employed fs laser experimental setup used to reduce the oxygen functional groups is discussed in details in section 3.2. In section 3.3, the three utilized thin film fabrication techniques that were used in this research are described. Finally, section 3.4 discusses the molecular characterization platforms used including Raman spectroscopy, X-ray photoluminescence, X-ray diffraction analysis. FTIR spectroscopy and UV-VIS spectroscopy. The experimental procedures of rGO films surface morphology and electrical properties are also described in this section.

3.2.1 Laser specifications and properties

Two different fs-laser systems with different pulse duration and pulse energy were used in this research. The first system was a homemade fs laser pulses generated from a Ti: Sapphire ultrafast regenerative amplifier with operating wavelength of 800 nm, pulse duration of 75 fs, repetition rate of 1 kHz and pulse energy of 250 μJ. The second one was fs laser system from spectra Physics Millenia with operating wavelength of 800 nm, pulse duration of 35 fs, repetition rate of 1 kHz and pulse energy of up to 4 mJ were used as light source in this research. The laser pulses are generated from the Ti:Sapphire jewel oscillator using regenerative amplifier and the Quantronix pulse generator which includes pulse shaper, chirped mirrors, stretcher and the prism compressor as shown in Fig.3-1
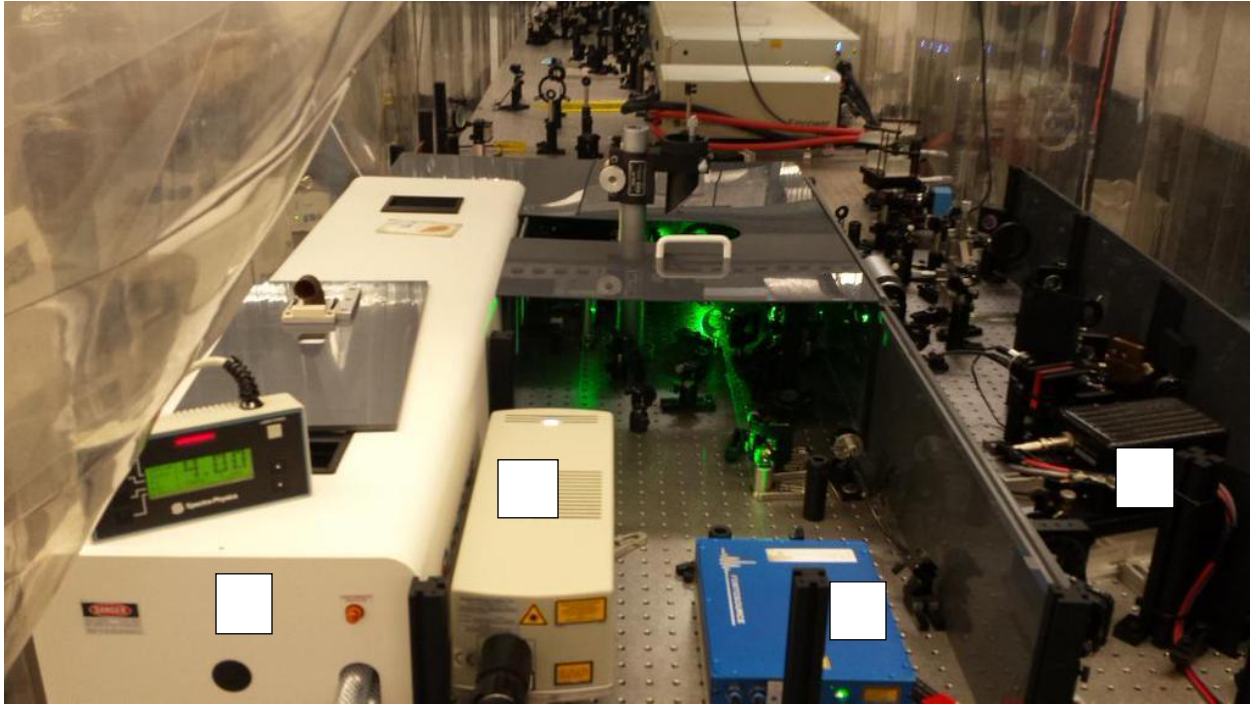
Figure 3-1: (a) Spectra Physics Millenia 4W. (b) Oscillator75 MHz (c) Quantronix pump laser 1 kHz. (d) Regenerative Amplifier.

Fig.3-1 and Fig.3-2 show the fs laser setup and experimental setup respectively that were used in this research. The incoming laser beam was reflected downwards using a concave silver coated mirror. The

24

incident laser beam was passed by a convex focal lens and focused at the surface/inside of the aqueous solution as shown in Fig.3-2a. The beam focal point was placed at different distances from the liquid establishing long and short focal length of 10 cm and 5 cm respectively. A wide range of exposure time and pulse energy in the range of 250 µJ to 2 mJ were controlled using iris diaphragm (Fig.3-2b).
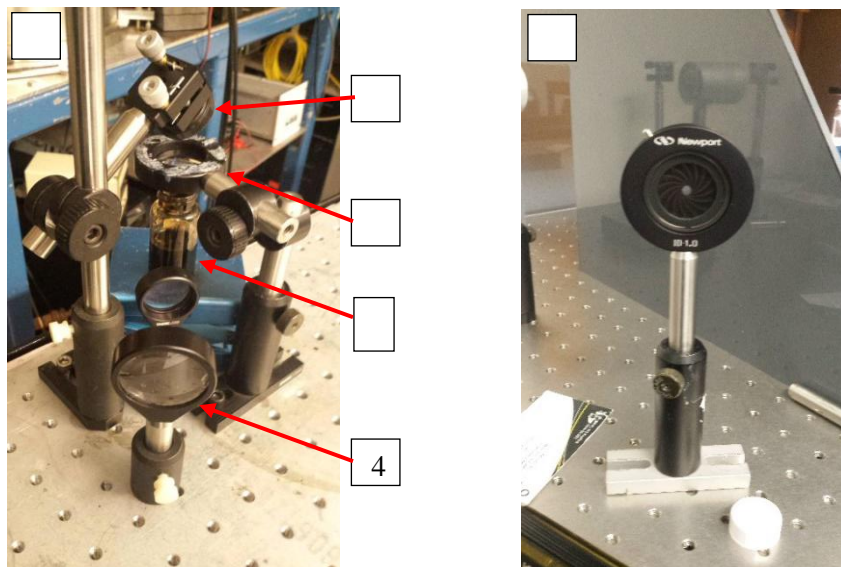
Fig. 3-2: (a) Laser exposure setup, 1: Dielectric mirror directing the incident beam into the solution (graphene oxide), 2: focusing lens with different focal length, 3: Silica vial containing the graphene oxide solution, 4: Double magnification lens used for footage-capture purpose. (b) Iris diaphragm used for manipulating the beam diameter and the laser beam energy.

3.2.2 Laser – Graphene oxide solution interaction

Two different experimental setups were used in this research; in the first setup, the laser beam was focused few millimeters inside the solution surface, whilst in the second setup the laser beam was focused at the air/GO interface. Both of which will be discussed thoroughly in the upcoming sections.

3.2.2.1 Under surface exposure

The laser beam was focused few millimetres inside the GO solution using a convex lens with focal length of 5 cm. By focusing the laser beam inside the solution, a white filament of 1 mm length was observed as a result of the ionization [58]. The effect of observing this filament was reported as increasing the interaction volume by three orders of magnitude given the spherical focal point under the solutions surface, while capping the intensity at around 4×10^{13} W/cm^2 [58, 59]. The spherical focal point was approximated to be 25 micrometer in diameter, whereas smooth bubbling was formed below the surface
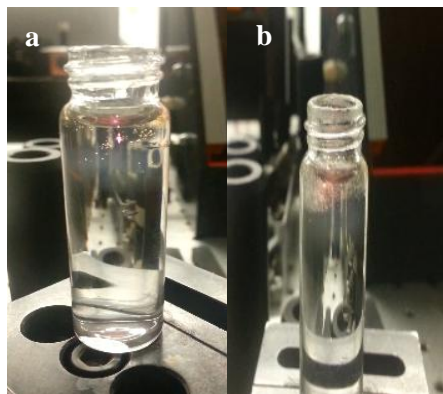
as a result of the interaction with the solution as shown in Fig.3-3a.

Figure 3-3: Laser focal point (a) below the surface of the solution and (b) at the air/solution interface (water was used for its transparency to ease illustration purposes).

3.2.2.2 Surface Exposure

In this technique of exposure, the incident beam was focused at the air/solution surface interface as shown in Fig.3-3b.

By using surface exposure, several effects such as liquid turbulence, disordered bubbles and most importantly liquid vaporization were observed as shown in Fig.3b. These phenomena can be attributed to the high photon energy interacting with different material, (4×10^{19} W/cm^2).

3.3 Film fabrication

A series of thin films were fabricated from exposed solutions both using surface and under surface exposure techniques, to study the effects of changing the laser parameters on the material's, chemical and physical properties of reduced graphene oxide solutions. Three different methods of film fabrication were utilized in this study. Thin films were fabricated using the spin coating mechanism whereas thick films were fabricated using drop casting technique. In both techniques, silicon wafer was used as substrate.

3.3.1 Spin-coating technique

The rGO and GO thin films were fabricated using spin casting technique with speed of 3000 rpm for 30 seconds followed by 20 min post-baked at 90 ^{o}C in order to relief thermal stress and increase the adhesion between the film and substrate. The fabricated thin films then was naturally cooled down to room temperature.

3.3.2 Drop casting technique

Thick rGO films were fabricated by using drop casting technique. In this technique, a drop (usually less than 1 mL) of the rGO solution was placed on the silicon substrate and left at room temperature to dry and evaporate the water content in the sample. The advantages of the drop casting technique is that it is very simple and consumes very little amount of liquid. Some drawbacks of such method of film fabrication include lack of homogeneity and difficulty of controlling the film thickness. This method was useful for characterization tools that did not require a certain thickness, and homogenous film such as AFM and SEM, where the focus was centered towards investigating the morphology and characteristics of the rGO flakes.

3.3.3 Free standing film fabrication

Freestanding rGO and GO thin films were fabricated using vacuum filtration [60] . A Whatman Anodisc filter membrane of 0.05 μm pore-size was mounted on a simple vacuum system operated by means of a buchner funnel and flask (Fig.3-4a), whereas a small volume of the exposed rGO solution was applied gently on the filter membrane to ensure the water content is vacuumed through the openings of the filter pores. The membrane was then baked for 6 hours at 50 degree Celsius inside an oven to evaporate any excess water within the filtered film (Fig.3-4b). Separation of the membrane filter was carried out by means of etching in hydrochloric acid (Fig.3-4c). The film was then lifted from the hydrochloric acid
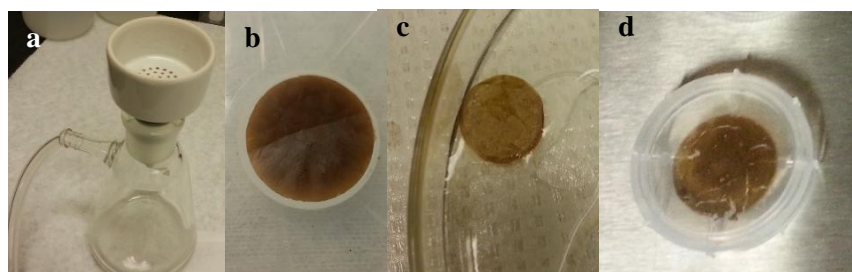
(etching solution) and kept to dry as shown in Fig.3-4d.

Figure.3-4: (a) Buchner funnel and flask connected to vacuum system, (b) Filtered film on the membrane after post oven baking and (c) etched rGO free standing film from membrane in HCl and (d) film after being lifted from the etching medium and left to dry.

3.4 Characterization and spectroscopy

Several characterization methods such as XPS, XRD, Raman, FTIR and UV-VIS spectroscopy were employed to study the effects of different infrared exposure parameteres on the physical, electrical, chemical and material properties of the rGO and GO solutions. Geometrical characterization such as determination of the number of layers and their thickness, surface roughness and surface morphology of high quality rGO films were also carried out using SEM, AFM and TEM.

3.4.1 Absorption spectroscopy

Graphene oxide chemically consists of sp^2 bonded carbon, accompanied with oxygen functional group in-plane and on the edges of the graphene sheets. Therefore, it is crucial to understand how the GO solutions and films behave from a chemical point of view within context of several experiments. Fourier transform infrared spectroscopy (FT-IR) 8400S spectrometer from Shimadzu in the range of 500 cm^{-1} and 4500 cm^{-1} was carried out to investigate the vibrational frequency and molecular structure of the GO and rGO films. Since some carbonyl bonds are not excited in the IR range, the UV Visible (UV-2501PC) spectrometer from Shimadzu was used at resolution of 0.5 nm and medium scanning speed in the range of 190 nm to 1100 nm.

3.4.2 Molecular analysis

X-ray photo-lumionancse spectroscopy (XPS) is a powerful technique to detect various oxygen functional groups. Decovolution of C1s peak of graphene oxide enables a preview study of the effects of changing the exposure parameters such as laser energy, pulse duration and pulse focal point on the molecular and chemical structure rGO.

The XPS was carried out using Thermo ESCALAB 250 instrument configured with a single wavelength AlKa X-ray source with incident energy of 1486.6 eV and power of 150 W. The analysis chamber base pressure was $< 3 \times 10^{-10}$ mbar and data were collected using electron beam energy of 20 eV for the core-shell spectra and 50 eV for survey spectra. The takeoff angle, which is defined as the angle between the substrate normal and the detector, was fixed at 0 degree. The CasaXPS software was used for XPS spectrum analysis. Energy dispersive x-ray spectroscopy (EDX), was also used to characterize the type of elements available within the sample.

Raman spectroscopy is one of the common non-destructive tools used to characterize graphene [61]. A measure of the levels of defect of the graphene oxide sample and the quantifying of the number of layers can be obtained by recording the Raman spectrum of rGO and GO[31] . The Raman spectrum of rGO and

GO thin films were recorded using a Reinshaw micro-Raman spectrometer using excitation wavelength of 632.8 nm and power of 20 mW.

Reduction of graphene oxide aims primarily to remove the oxygen functional groups located at the periphery and in-plane of the graphene networks, therefore X-Ray diffraction analysis (from X'Pert Panalytical) was also carried out to calculate the interlayer spacing between the graphene sheets and their crystallinity structur. Thus the success of removal of some of the oxygen functional groups (specifically the OH radicals) can be confirmed recording the XRD spectrum [34].

3.4.3 Surface Morphology

Investigation of the surface morphology was accomplished primarily using atomic force microscopy, AFM, (Dimension 3100 Scanning Probe Microscope) providing quantitative analysis regarding the graphene oxide flake's roughness, vertical distance and lateral dimension. Scanning electron microscope, SEM, (Leo 1530 SEM) also offer high resolution and view the surface morphology and stacking of the GO layers. To better understand the layering of the graphene oxide sheets, Zeiss Libra 200MC transmission electron microscope (TEM) was also used where the aggregation of the graphene oxide networks was of interest.

3.4.4 Electrical properties

Graphene and graphene oxide is largely used in electrical applications such as transistors, photo-detectors and sensors. Therefore its electrical properties such as sheet resistance and conductivity play an important role in GO based devices. In this research, the effects of changing the exposure parameter on the electrical conductivity of the rGO films were studied using the 4-point probe-lock Keithley 4200-SCS semiconductor characterization system.

3.5 Summary

Aiming to address the objectives of this study, graphene oxide suspended in aqueous solution was manipulated using fs laser with different, laser pulse energy, laser focal point position, focal length, different pulse duration, different exposure time, and using different concentrations of graphene oxide solution. The variation of fs laser parameters and GO concentration in the aqueous solution, all yielding various color, textures and properties to the solution. A series of thin films were fabricated using three differnet techniques; spin coating of thin films, drop caasting of thick films and vacuum filteration (for free standing films). Therefore, in the upcoming chapters and sections the physical, chemcial, electrical and material properties of the afore mentioned film will be discussed in details.

Chapter 4

Ultrafast laser interaction with low and high concentration graphene

_____

_____

4.1 Introduction

In this chapter, the laser treatment of low (GO1) and high (GO2) concentration graphene oxide will be analyzed comprehensively. The fs laser of which specifications were described in Chapter 3 was employed to expose the 5 mL of graphene oxide aqueous solution in a 7 mL quartz tube. This chapter will discuss the UV visible, XPS and Raman spectroscopy analysis to investigate the molecular structure of the yielded GO solutions. Surface morphology and electrical properties of the obtained solutions will also be studied.

4.2 Experimental Procedure

The laser energy and focal length that were used to treat the GO1 and GO2 solutions were 250 µJ and 5 cm respectively. The utilized concentrations for GO1 and GO2 were 0.5 mg/mL and 6.2 mg/mL,

respectively. The exposure time for both solutions varied in the range of 0.5 hrs to 6 hrs and rGO1 and rGO2 thin films were fabricated by means of spin casting technique using the acquired solutions.

The exposure process was found to turn the graphene oxide solution color from a pale yellow to a dark brown and finally a black color over the 6 hour interval, providing preliminary visual evidence of the success of the reduction process [44] as shown in Fig. 4-1. This turn in color was indicative of the restoration of the sp^2 bonded carbon network [47]. The focal point was placed under the surface by a few millimeters as explained in section 3.2.2.1.
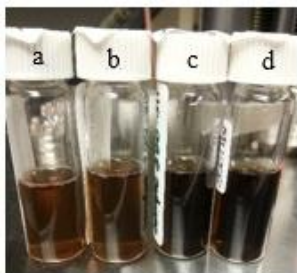
Figure 4-1 : Low concentration graphene oxide solution after exposure to ultrafast laser (λ=800 nm and energy density of 4.45×10^5 mJ/cm^2) for a) 30 min, b) 60 min, c) 3 hrs and d) 6 hrs.

4.3 Reduced low and high concentrations graphene oxide aqueous solution characterization.

4.3.1 Molecular bond analysis

4.3.1.1 UV-Visible spectroscopy

The UV visible spectrums for both rGO1 and rGO2 are shown in the figures below. The two main absorption peaks were recorded at 230 nm and ~300 nm. The absorption peak at 230 nm was attributed to $\pi \rightarrow \pi^*$ transition in the C=C molecular bond [34]. As can be seen from Fig.4-2a, a gradual increase in the whole spectral region for all the C=C absorption bond was recorded as results of laser exposure compared to the unexposed (0 hrs) spectrum. This could be attributed to the restoration of the C=C bonds and π networks. It was also found that by increasing the exposure times, the absorbance intensity was decreased, which was due to the production of more hydroxyl groups within rGO1 sheets. In the rGO2 solution the C=C peak was redshifted by 20 nm and was recorded at wavelength of 250 nm, which could be due to the difference in concentration of host material (water) and the randomness of the carbon

33

configuration and the different type of orbital hybridization [62]. From Fig.4-3b, it is also clear that FWHM of the C=C peak was larger than that one in Fig.4-2.a, which is a result of the carbon saturation effect in the GO2 and rGO2 solutions. The n→π* transitions in the carbonyl groups C=O was recorded at wavelength of 300 nm as shoulder for both rGO1 and rGO2 [32]. It was found that by increasing the exposure time from 0 to 6 hrs, the FWHM of the n→π* transitions in the rGO1 was increased that was attributed to the reduction of carbonyl (C=O) molecular bonds, as it is clear from Fig.4-2a.
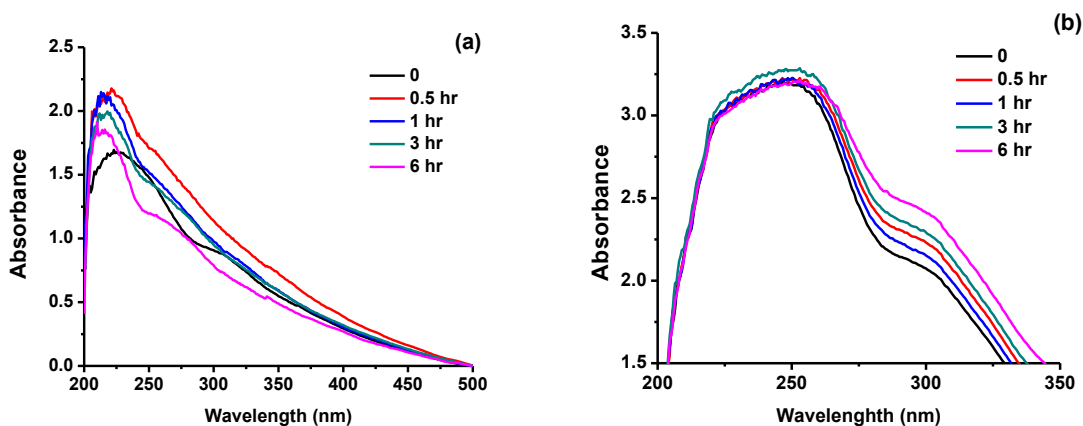
Figure 4-2: The recorded UV-VIS spectrums for (a) rGO1 and (b) rGO2 in the wavelength range 200 nm to 500 nm.

Energy dispersive x-ray (EDX) method was utilized to investigate the effects of variation of exposure time on the chemical concentration of the elements within the samples. Table 4-1 summarizes the effects of using different exposure time on the chemical concentration in weight percent of both carbon and oxygen elements in rGO1 and rGO2 solutions.

	GO1		GO2	
Exposure Time (hr)	Carbon (wt %)	Oxygen (wt %)	Carbon (wt %)	Oxygen (wt %)
0	65.01	34.99	77.74	22.26
0.5	68.31	31.69	86.46	13.54
1	64.03	35.97	86.32	13.68
3	67.55	32.45	85.00	15.00

| | 6 | 66.95 | 33.05 | 82.57 | 17.43 |

Table 4-1: The calculated elemental composition of rGO solutions in weight percent

It was found that the carbon concentration increased from 65.01 wt% to 68 wt% and from 77.74 wt % to

86.46 wt%, respectively in rGO1 and rGO2 solutions by increasing the exposure time from 0 to 0.5 hrs,

which can be also confirmed from UV-VIS spectra shown in Fig.4-2. It was also found that increasing the

exposure time from 0.5 hrs to 6 hrs, resulted in slightly more oxygen in both samples, which can be

attributed to the breaking sp^2 (C=C) bonds and production of active OH$^-$ radicals as it is detailed in Table

4-1. From this table it is also clear that, the carbon concentration of exposed GO2 solutions was larger

than that one in GO1 solution. This larger amount of carbon concentration confirms the afore mentioned

carbon saturation effect in the GO2 solution and therefore, 20 nm redshift of the $\pi \rightarrow \pi*$ transition as it

was shown in Fig.4-2b.

4.3.1.2 X-ray photoemission spectroscopy

The nature of the chemical bonds between the carbon and oxygen were studied by the XPS analysis of

fabricated thin films from both rGO1 and rGO2 solutions. Baseline correction and calibration was carried

out based on the Si2p transition at binding energy of 101 eV [63]. The recorded XPS spectra of both

exposed GO1 and GO2 solutions are compared in Fig. 4-4 and Fig.4-5 respectively.

The C-C binding energy for both GO1 and GO2 were recorded at 285 eV and 284.3 eV respectively,

whilst the oxygen functional groups were recorded at 287 eV, 288.7 eV and 290 eV attributable to C=O,

C-O and C-OOH bonds respectively in GO1 solutions [64-66]. A small shift of 1 eV to 2 eV in the

binding energy of C-O, C=O, C-O and C-OOH molecular bonds were recorded which could be attributed

to the experimental charging effect [67]. Fig.4-4a-c, show that intensity of the C-C molecular bonds of the

rGO1 was increased by increasing the exposure time from 0 to 1 hrs. From these figures it is also clear

that oxygen functional groups peaks were reduced which can be attributed to the successful reduction

process at this point. Furthermore, increasing the exposure time from 1 hrs to 6 hrs resulted in no

significant increases in the C-C molecular bond intensity compared to the C-O molecular bond (Fig.4-4c-e). As can be seen from Fig.4-4d, after 3 hrs exposure the intensity of the oxygen functional groups features (i.e. C-O, C=O and C-OOH molecular bonds) was increased which was accompanied by decreases in the C-C molecular bond intensity. This could be attributed to the production of carbon atoms with lone pairs electrons and hence yielding more amount of hydroxyl and carbonyl groups and resulting in the sp^3 hybridization enhancement as a result of more oxidation of the graphene sheets.

The recorded XPS spectra for rGO2 solutions are shown in the Fig.4-5. It was found that the C-C peaks were increased as a result of the exposure process from 0 to 1 hrs. However, the C-C bond peak intensity was decreased by increasing the exposure time from 3 hrs to 6 hrs which was accompanied by increasing the intensity of the oxygen functional group that can be attributed to the disassociation of the C-C bond and introduction of the oxygen atoms into the graphene sheets.
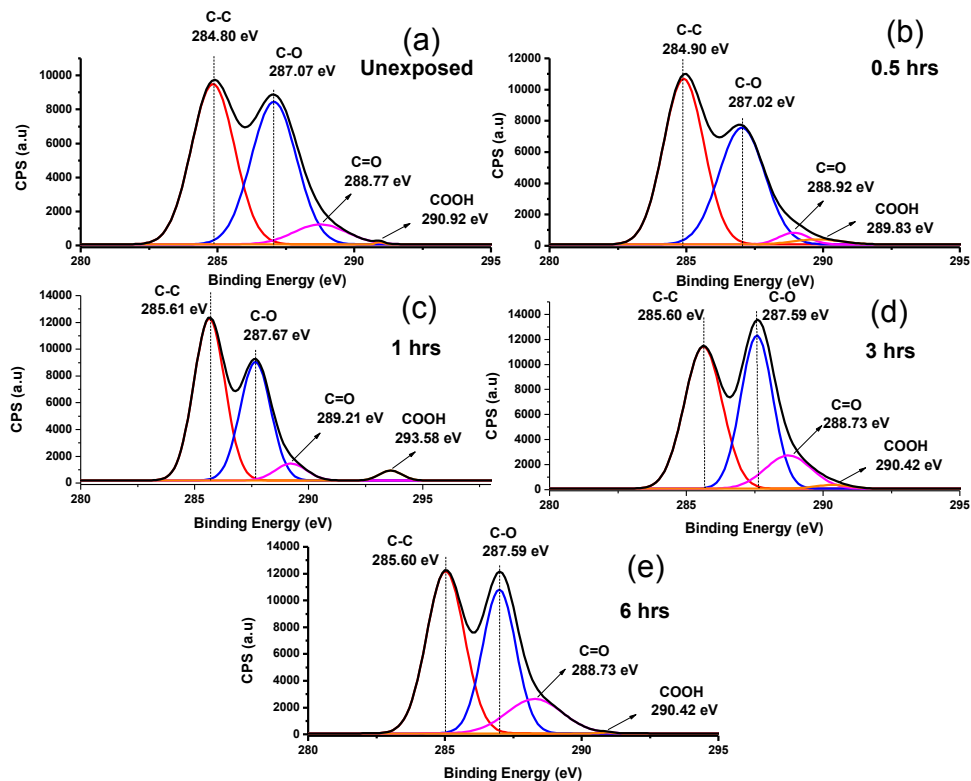
Figure 4-3: The recorded XPS spectra of GO1 solutions at different exposure time of a) 0, b) 0.5 hrs, c) 1 hrs, d) 3 hrs and e) 6 hrs.

Table 4-2 summarizes the C-O atomic ratio and the FWHM both rGO1 and rGO2. It was found that the C-O ratio was increased by 1.10x and 3x for both GO1 and GO2 respectively after 6 hrs exposure as summarized in Table 4-2. As it is clear from this table, the laser treatment resulted in more effects on the GO2 rather than GO1 in terms of reducing the oxygen functional groups, which is due to the concentration difference (ratio of H_2O to graphene oxide flakes).

It was also found that the FWHM of the C1s and O1s transitions was decreased due to the exposure time increases from 0 to 1 hrs. However, further increasing the exposure time to 6 hrs leads to gradual increases in the FWHM of C1s transition from 3.7 eV to 3.96 eV and 1.99 eV to 3.7 eV for both rGO1 and rGO2, respectively. The FWHM of the O1s transition was also increased from 2.41 eV to 2.51 eV and from 1.80 eV to 2.07 eV respectively in both rGO1 and rGO2 solutions, as it is detailed in Table 4-2. These variations in FWHM values of O1s and C1s transitions could be attributed to more production of carbonyl bonds.

Table 4-2: The atomic ratio and fs-laser exposed solution. The wavelength, pulse energy and were fixed at 800 and 1 kHz, calculated C/O FWHM values of GO1 and GO2 exposure duration, pulse repetition rate nm, 75fs, 250µJ respectively.

| Exposure time (hrs) | C1s/O1s | | FWHM (eV) | | | |
| | | | C1S | | O1S | |
	GO1	GO2	GO1	GO2	GO1	GO2
0	2.32	0.53	4.538	1.914	2.829	1.852
0.5	2.25	0.74	3.886	1.843	2.787	1.821
1	2.15	0.45	3.702	1.992	2.410	1.809
3	2.55	0.60	3.912	1.808	2.440	1.824
6	2.56	1.60	3.963	3.703	2.510	2.073
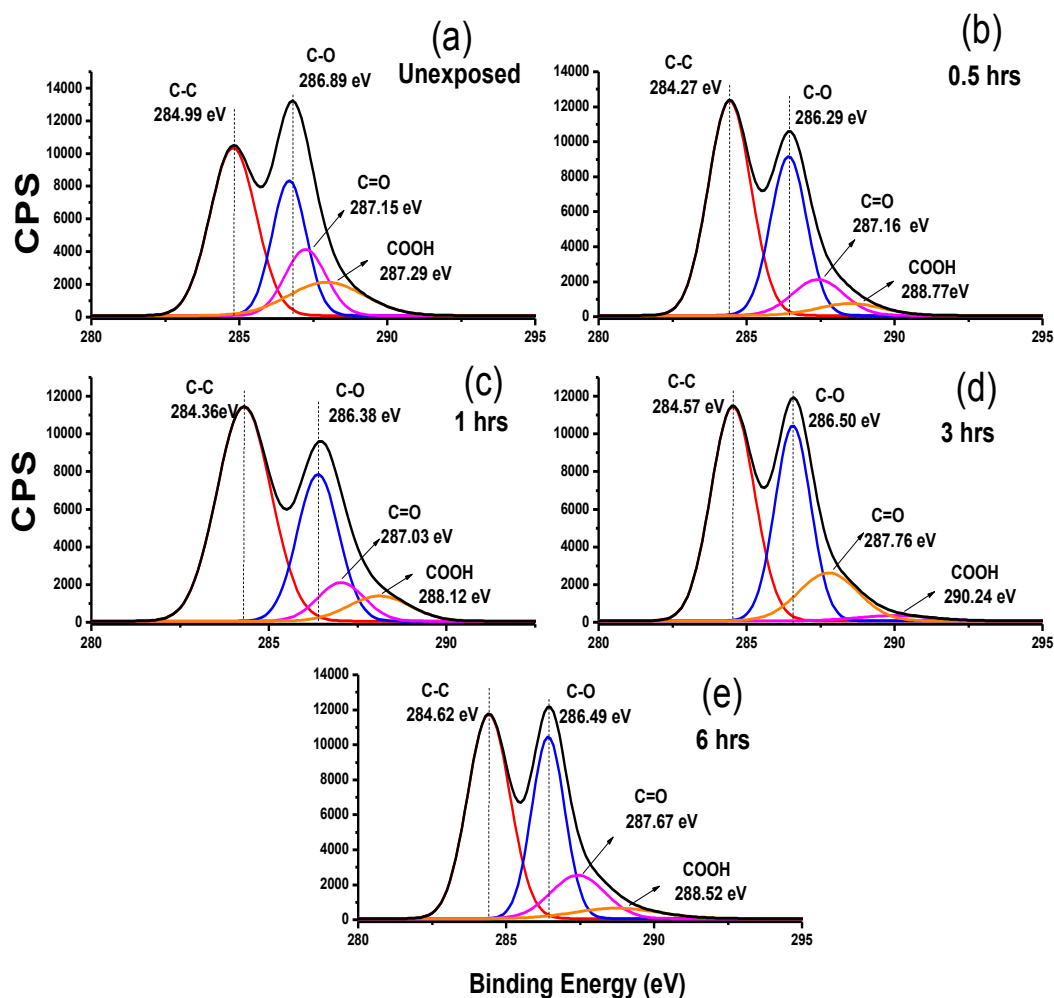
Figure 4-4: The recorded XPS spectra of GO2 solutions at different exposure time of a) 0, b) 0.5 hrs, c) 1 hrs, d) 3 hrs and e) 6 hrs.

4.3.1.3 Raman spectroscopy

Fig.4-5a and Fig.4-5b show the Raman spectra of both unexposed and exposed GO1 and GO2 solutions. Two main recorded Raman peaks that were assigned to the D and G bands were recorded at wavenumber of 1329 cm^{-1} and 1588 cm^{-1} respectively. The D peak in both GO1 and GO2 solutions was recorded due the existence of sp^3 carbon decorating the periphery of the graphene oxide basal plane acting as defects. It can be concluded, that the D band was recorded as a result of the breathing mode of the sp^2 bonded atoms in the carbon ring [68]. The G band was recorded due to the disordered linkage between sp^2 and sp^3

38

carbon atoms [69]. As can be seen from Fig.4-5a, two weaker peaks were recorded at wavenumber of 2663 cm^{-1} and 2894 cm^{-1} which were assigned to 2D and D+G combination bands respectively [70, 71].
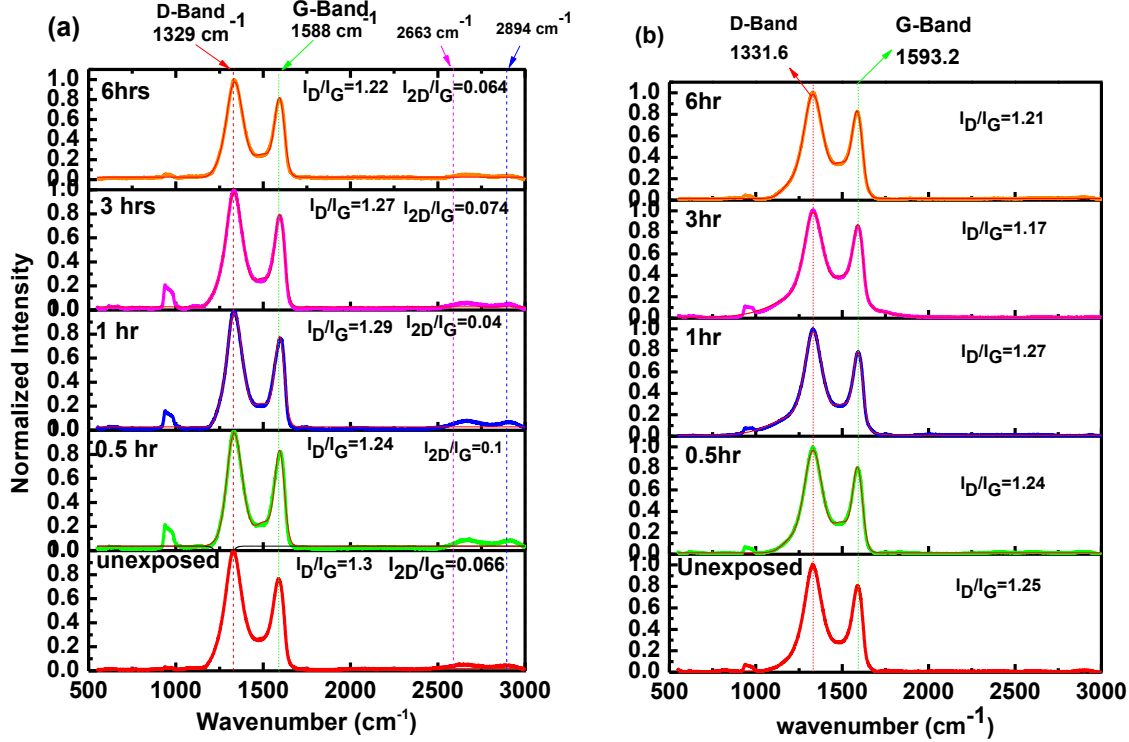
Figure 4-5: The recorded Raman spectra of rGO1 and rGO2 thin films. The excitation wavelength and power was 632.8 nm and 20 mW respectively.

As it is clear from Fig. 4-5b, the recorded G band position was slightly shifted towards larger wavenumber which is due to the reduction of the graphene oxide flake thickness [68] in the rGO2 thin films.

The quality of the deposited rGO thin films were investigated by studying the defect ratio which is calculated from I_D/I_G [68]. From Fig.4-6 it can be seen that the I_D/I_G ratio of both rGO1 and rGO2, was increased by increasing the exposure time from 0.5 hrs to 1 hrs which can be attributed to the π-orbital misalignment as a result of the 1 hrs exposure. Further increasing the exposure time to 6 hrs resulted in the gradual reduction of the I_D/I_G ratio and minimum ratio of 1.22 and 1.21 was calculated for rGO1 and rGO2 respectively.
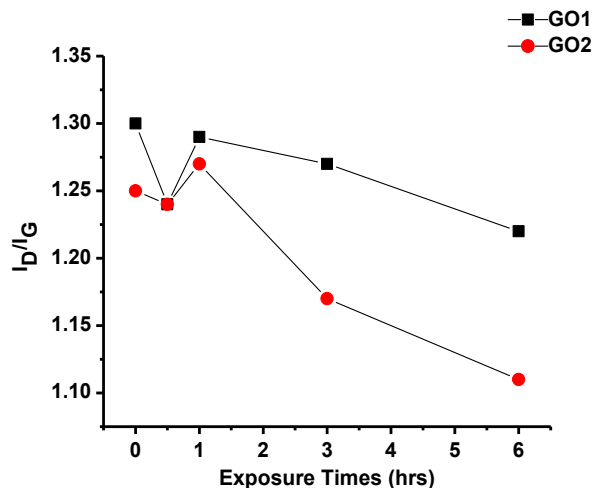
Figure 4-6: Calculated I_D/I_G ratio as a function of exposure time of both GO1 and GO2 solutions

From Fig.4-6 it can be seen that the D band is more intense than the G band which occurs as a result of the sp^3 hybridization bonding enrichment due to the laser treatment. The transition from sp^2 to sp^3 was acquired as a result of the introduction of the oxygen atoms into the basal plane of the carbon networks or hydroxyl groups in the out-plane direction via chemisorption.

4.3.2 Surface morphology

The surface morphology of the fabricated thin films for both GO1 and GO2 thin films were investigated using AFM as shown in Fig.4-7. The measured average roughness and vertical distance of graphene flakes were reported in Table 4-3. It was found that the average roughness of the rGO flakes was reduced from 54.53 nm and 4.97 nm to 18.85 nm and 0.219 nm for rGO1 and rGO2 respectively after 6 hrs of laser treatment. A significant reduction of 70 % and 85 % was also recorded in the vertical distance of the rGO1 and rGO2 respectively after 6 hrs of exposing the GO aqueous solutions. This reduction in average roughness of the rGO flakes and vertical heights could be due to the reduction of the irregularity of the flakes surfaces. From Table 4-3, it is also evident that the surface roughness improvements in the rGO2 thin films was much larger than that in the rGO1 films. It was also found that the lateral dimension of the studied rGO flakes was significantly reduced as flake roughness was improved in rGO2 films.
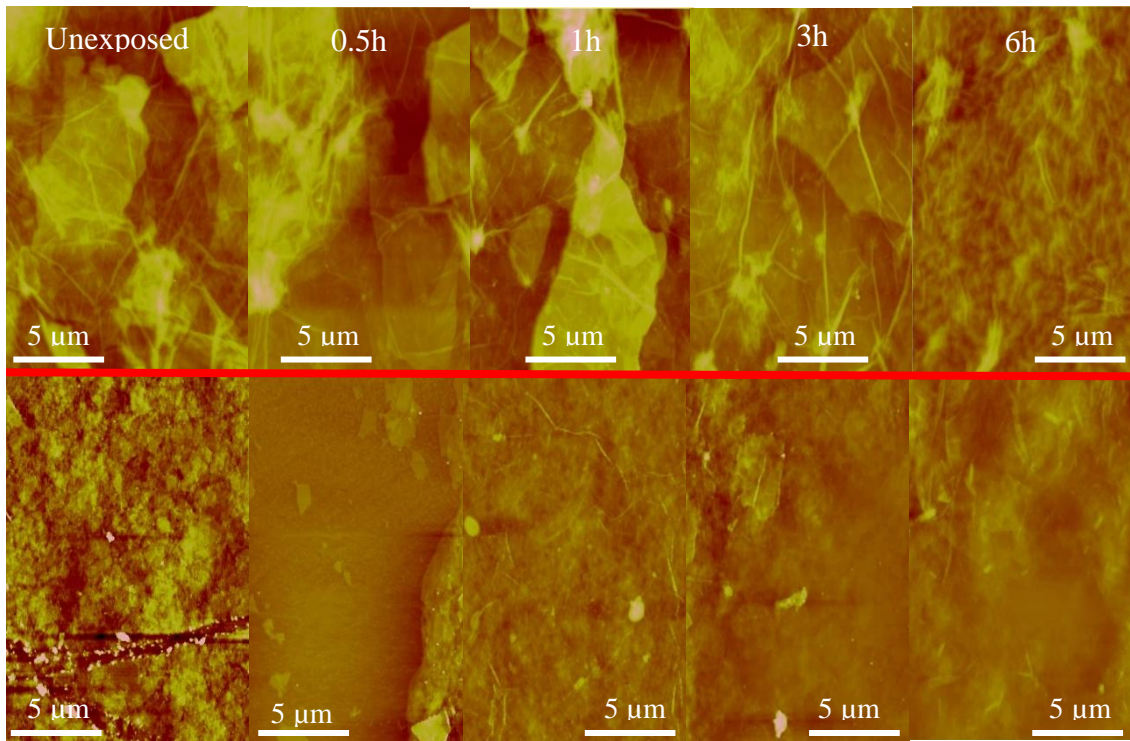
Figure 4-7: The AFM images of rGO1 (top row) and rGO2 (bottom row). The scanning region was 15 µm×15 µm.

Table 4-3: The surface roughness of the rGO1 and recorded average and vertical height rGO2 flakes.

Exp. time (hrs)	Ave. roughness (nm)		Vertical height (nm)	
	rGO1	rGO2	rGO1	rGO2
0	54.53	4.975	96.18	10.42
0.5	40.89	0.84	75.41	2.51
1	38.84	0.86	65.64	2.42
3	21.07	0.389	41.68	2.11
6	18.85	0.219	28.84	1.61

SEM images of both unexposed and 6 hrs exposed rGO1 and rGO2 thin films are shown in Fig.4-8. As it is clear from Fig.4-8.a, the unexposed GO1 films offer an isolated regions of graphene flakes with large lateral dimensions as indicated in Fig.4-8a. The isolated graphene flakes was acquired due to high level of dilution of the GO1 solutions (0.5 mg/mL) compared to the GO2 solutions. It was found that after 6 hrs
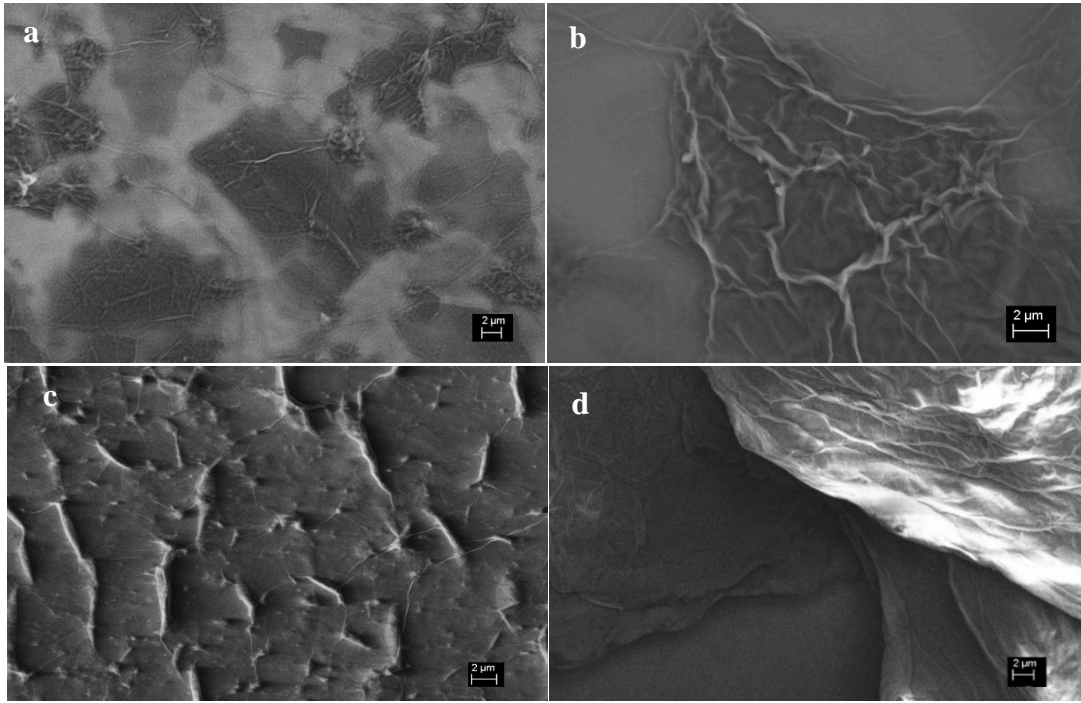
exposure a series of large cluster of linked graphene oxide flakes (~13 μm x13 μm) that comprised with wrinkled features were acquired by merging the isolated flakes as shown in Fig.4-8b

Figure 4-8: The SEM images of (a) and (c) unexposed and (b) and (d) after 6hrs exposure GO1 (top row) and GO2 (bottom row) thin films

As it is shown in Fig.4-8c, the unexposed GO2 thin films offers a smoother surface than that in the rGO1 films, whereas the 6 hrs exposed GO2 thin films show aggregated graphene oxide sheets over each other to form stacked layers as it is clear from Fig.4-8d. From this figure, the structural layer of GO sheets can also be seen which is due to the van der Waal forces between the GO sheets and hence increases the carbon-carbon bonds followed by reduction of the oxygen functional groups especially the hydroxyl bonds within rGO2 films [72].

4.3.3 Electrical properties

Four point lock-in technique was used to calculate the sheet resistivity of the rGO1 and rGO2 fabricated thin films. Fig.4-9a shows the sheet resistivity of both rGO1 and rGO2 freestanding films as a function of the exposure times. As it is evident from this figure, the sheet resistivity was significantly decreased by 22

% on increasing the exposure time from 0 to 6 hrs in rGO1 whereas the sheet resistivity reduction was recorded by 2.9 % in the rGO2 films as results of 6 hrs laser treatment.

The resistivity of graphene oxide freestanding films and rGO by means sun light, UV light, excimer laser at 248 nm wavelength [30] and the utilized fs laser at wavelength of 800 nm, pulse energy of 250 µJ and pulse duration of 75 fs and repetition rate of 1 kHz are compared in Fig.4-9b. As can be seen from this figure, GO (GO1 and GO2) reduced by fs laser pulses offers 4 orders of magnitude lower sheet resistivity compared to acquired rGO by using nanosecond laser pulses (248 nm wavelength). The decrease in the value of the sheet resistivity could be attributed to the low heat diffusion of the laser during exposure process, and therefore the thermal effects acquired by the fs laser process was recorded much smaller than UV light and ns laser pulses treatment as discussed in details elsewhere [30, 73].
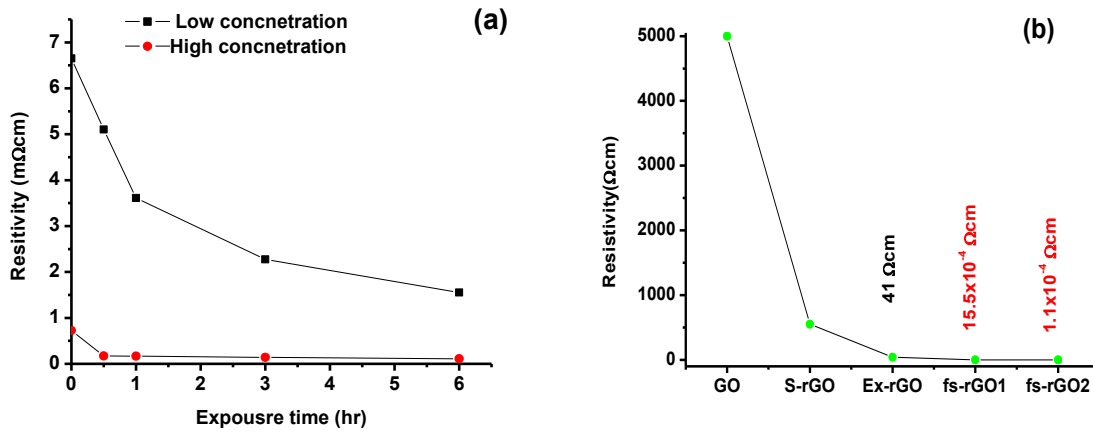
Figure 4-9: (a) Sheet resistivity as a function of exposure time and (b) typical sheet resistivity values of reduction methods [30].

4.4 Summary

Fs laser pulses were used to expose two different concentration of GO aqueous solutions. By placing the beam focal point under the surface of the solution by few millimeter and employing pulse energy of 250 μJ the solutions were treated for 0.5, 1, 3 and 6 hrs.

The UV visible spectra show an increase in the absorption spectral region for both rGO1 and rGO2 compared to unexposed spectra. The reduction in the absorbance intensity for the C=C transition accompanied with the presence of the C=O bond suggested that oxygen atoms were being introduced by increasing the exposure time that resulted in decreasing the C=C bond. This was also confirmed by EDX, where the carbon weight percentage was found to increase to its maximum values after 0.5 hrs of exposure before slightly increases of oxygen weight parentage. The XPS analysis also confirmed the aforementioned analysis by showing an increase in the oxygen related bonds specifically the C-O, this was consolidated when the Raman spectroscopy showed an enhancement in the sp^3 hybridization. However, the electrical resistivity were found to massively decrease as a result of the 6 hrs exposure, which indicates the success of the reduction process on the enhancement of the electrical properties of GO.

Surface morphology studies indicated the increase of the flake size (in AFM) and the aggregation of the flakes to increase the surface area of the flakes as stated by the UV Vis analysis regarding the restoration of the C=C bonds.

Chapter 5

Graphene oxide sol-gel fabrication via ultrafast laser interaction

_____

5.1 Introduction

5.2 Experimental procedure

5.3 Graphene oxide sol-gel Characterization

        5.3.1 Absorption spectroscopy

        5.3.2 X-ray photoemission spectroscopy

        5.3.3 Raman spectroscopy

        5.3.4 Surface morphology

        5.3.5 X-ray diffraction analysis

5.4 Summary/Conclusion

_____

5.1 Introduction

In this chapter, a novel technique of graphene oxide sol-gel (GOSG) fabrication will be introduced where it is systematically analyzed. High concentration graphene oxide aqueous solution (6.2 mg/mL) was employed in a novel fabrication technique, where the 2-dimensional graphene oxide sheets assemble GOSG via supermolecular π-π interactions using fs laser ablation technique discussed in section 3.2.2.2, to evaporate the water content from the aqueous GO solution. Significant reduction of water content in the exposed GO solution consequently brings the 2-dimensional graphene sheets together in vicinity due to electrostatic interaction and weak van der Waal forces and hence creating the viscous GOSG [74]. This method is advantageous in the sense that no chemical mixing/treatment [75] and prolonged thermal treatment take place [76], which can affect the structural integrity of the graphene sheets.

In this method high concentration GO aqueous solution was exposed by fs laser pulses with pulse energy of 250 µJ and 2 mJ, pulse duration of 75 fs and 35 fs, repetition rate of 1 kHz and wavelength of 800 nm. The chemistry behind graphene oxidation is based on the oxygen functionalization with carbon atoms in the hexagonal networks, whereas oxygen functional groups such as (-OH, O and –COOH) generally considered as defect sites and decorating the periphery of the graphene planes [77]. These oxygen functional groups and water molecules dispersed in all directions disrupting the pure hexagonal structure of the carbon basal plane.

This study was based on the method of which the laser exposure was undertaken. In this case, GOSG was assembled in a manner where the incident beam was focused at the air/solution interface, thereby creating an excited white filament in the air that ends at the surface of the GO solution [59]. The incident beam focusing position plays a crucial parameter in the formation of GOSG. As a result, by focusing the laser pulses at the air/surface interface abundance of turbulence was created resulting in vaporization of the water content. The OH molecules which are sp^3 hybridized out of the basal plane covalent bonds have s character of 25 % which is lower than that of sp^2 hybridization (33% S character) [78], and therefore were decomposed and produced OH^- radical as a result of the high energetic laser pulses incident and hence yielded the water vaporization as shown in Fig.5-1b. After the appropriate exposure time, it was found that more than 50% of the volume of the solution was evaporated yielding a highly viscous solution with

(a)   (b)   (c)

(i)   (ii)
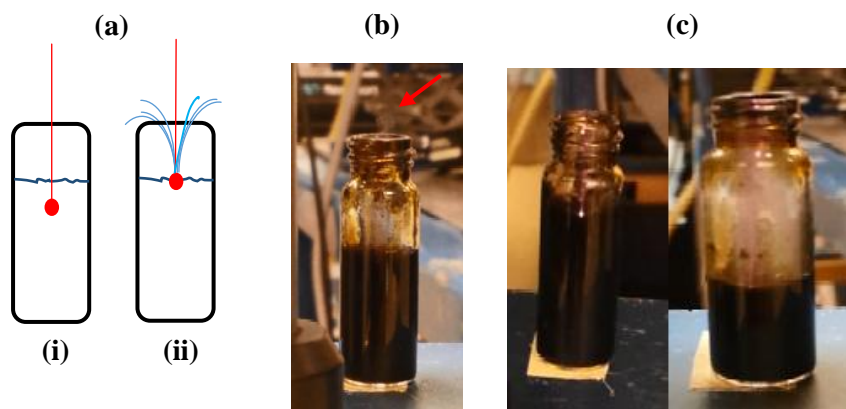
significantly less amount of water content as shown in Fig.5-1c.

Figure 5-1: (a) Schematic diagram of the exposure technique where (i) the incident beam was focused few millimeter inside the solution and in (ii) the incident beam was focused at the air/surface liquid interface resulting in the turbulent vaporization. (b) Vaporization exiting the vile (indicated with red arrow) into the atmosphere during the exposure process. (c) Graphene oxide volume at the beginning of the exposure process (left) and after completed exposure (right).

5.2 Experimental procedure

A quartz tube with 7 mL of aqueous graphene oxide solution with concentration of 6.2 mg/mL (from Graphene supermarket) was exposed to ultrashort laser pulses from the homemade fs laser setup. The incident beam was directed to the air/solution surface interface (discussed in section 3.2.2.) with a 5 cm focal length dielectric mirror. The GOSG was acquired after 7 hrs exposure. In order to reduce the GOSG production time various exposure parameters, such as incident beam focal length, pulse energy, pulse duration and initial volume of the GO solution, were manipulated to achieve the optimum exposure time. Using an initial volume of 4.5 mL and increasing the pulse energy to 2 mJ, pulse duration of 35 fs and increasing the beam focal length to 10 cm reduced the GOSG production time to 58 min rather 7 hrs.

Further optimization was carried out by further reducing the initial solution volume to 1.5 mL followed by altering pulse energy and incident beam focal length. It was found that GOSG was formed by using incident beam focal length of 10 cm, pulse energy of 2 mJ and 250 µJ and the GOSG was fabricated in 8 min and 16 min, respectively. Whilst, on using incident beam focal length of 5 cm and pulse energy of 2 mJ the GOSG was achieved after 20 min. The significant reduction of the GOSG production time could be attributed to the higher laser pulse energy and the manipulated parameters such as the different focal lengths, which resulted in longitudinal (large focal point) and compressed spherical focal point (small focal point) [58].

5.3 Graphene oxide sol-gel characterization

5.3.1 Absorption spectroscopy

Fig.5-2 shows the recorded FTIR transmission spectrum of unexposed GO thin films and the GOSG obtained at different exposure time. The dominant vibration fractures were recorded at 3381.46 cm^{-1},

1739.67 cm^{-1}, 1618 cm^{-1}, 1393.95 cm^{-1}, 1210.73 cm^{-1}, 1068.49 cm^{-1}, 835.11 cm^{-1} which are assigned to

the stretching OH, stretching C=O, C=C, C-OH, C-O-C, stretching C-O and the bending C-H [56, 74, 79,

80]. As can be seen from this figure the stretching OH valley offer larger deep for both 8 min and 16 min

exposed GOSG samples compare to that were obtained in the 20 min and 58 min. It was also found that

by increasing the exposure time to 7 hrs the OH absorbance feature was completely removed from the

FTIR spectrum, as it is evident from Fig.5-2. It can be concluded that, more exposure after GOSG

formation results in more OH bonds removal from the GOSG in the form of exiting vapor from the

volume container. It was found that the intensity of the sp^2 bonded C=O bonds were decreased for all the

GOSG solutions relative to the unexposed solution, which was due to more reduction of C=O bond as a

result of the fs laser exposure.
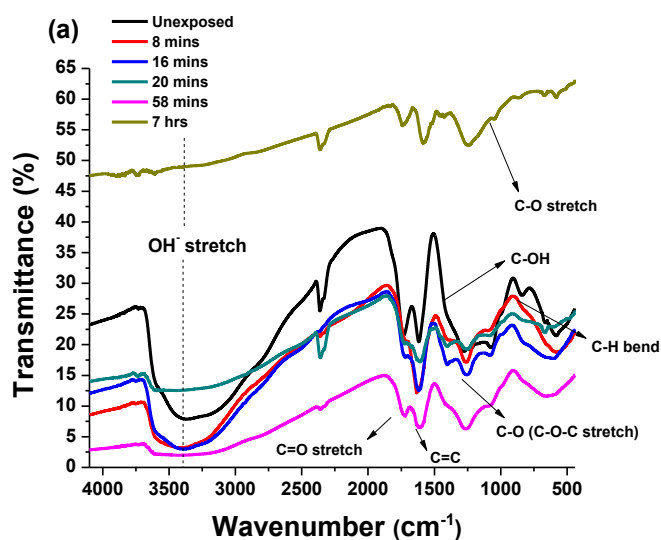
Figure 5-2: (a) The FTIR spectrum of unexposed GO thin film and fabricated GOSG in the different exposure time
in the range of 8 min, 16 min, 20 min, 58 min and 7 hrs.

From this figure, it is also clear that the sp^2 bonded C=C is still more prominent peak in all spectra. As

can be seen from Fig.5-2, it is clear that the C=C bond offers strongest absorbance for both 8 min and 16

min fabricated GOSG films which could be attributed to the lack of time for the laser to affect this bond

and hence the prominence of sp^2 C=C molecular bond. The absorbance intensity of the C-OH bond was

completely reduced in the GOSGs by increasing the exposure time. Whilst the amount of the bridging

oxygen between C atoms (C-O-C bond) becomes more prominent by increasing the exposure time, which can be attributed to the reaction of oxygen atom with two loan pair electrons with two carbon atom with single loan pair electron from broken C=C bond during the laser treatment. The bending C-H bond was disappeared in all of the GOSGs. This could be due to the dissociation of the weak sp^3 C-H bond and hence reactions between the hydrogen ions and free OH$^-$ ions and forming water vapor.

UV visible spectrum of GOSGs were compared in Fig.5-3. As can be seen from this figure the π→π* transition was recorded at wavelength of 233 nm which is attributed to the C=C bond [38]. The n→π* transition was recorded at wavelength of 300 nm, which is due to the C=O bond in the carbonyl groups[38]. It was found that lower exposure resulted in lower absorbance C=C transition and hence lower amount of sp^2 hybridization. It was found that the absorbance intensity of the 7 hrs GOSG was slightly decreased relative to the unexposed GO solution. However, as it is evident from Fig.5-3, the absorbance intensity of the C=O bond of the 7 hrs exposed GOSG was higher than that in the unexposed GO solution. This can be explained by the fact that free oxygen atoms/radicals reacted with free carbon atoms/radical after dissociation of the sp^2 C=C bonds, and hence producing more C=O molecular bonds.
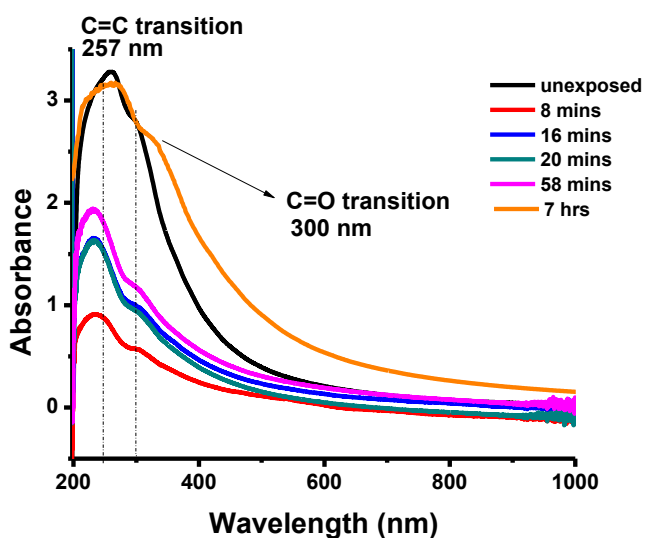
Figure 5-3: The recorded UV-VIS spectrum of GO and GOSG solution in the range of 200 nm to 1000 nm.

49

5.3.2 X-ray photoemission spectroscopy

X-ray photoluminescence spectroscopy (XPS) analysis was carried out to study the chemical structure of both carbon and oxygen atoms in unexposed GO and GOSGs. In Fig.5-4 the XPS spectrum of the C1s peak of both unexposed GO and GOSGs are compared. As can be seen from this figure, multiple peaks can be fitted in to the C1s transition which were corresponded to C-C, C=C, C=O and C-O at binding energy of 284.5 eV, 285 eV, 287.2 eV, 288.5 eV respectively [81].

It was found that the 7 hrs GOSG yielded four different peaks similar to the unexposed GO. As it is clear from Fig.5-4 the intensity of the C=C peak was decreased compared to that unexposed GO film. This is accompanied with increases in the intensity of the C-O peak, which is due to more production of the sp^3 hybridization features by dissociation of the sp^2 bonds as a result of the 7 hrs laser treatment. It was also found that the C1s transition in the 58 min , 20 min , 16 min , and 8 min GOSG comprised only three peaks namely C-C, C-O and C=O bonds, where the COOH and C=C peaks were absent compared to the unexposed solution and 7 hrs GOSG respectively. This could be attributed to the presence of the oxygen functional groups on the edges of the graphene sheets rather than the center. The presence of the oxygen atoms on the periphery of the graphene sheets helps in the aggregation of the GO sheets by means of the oxygen bridging and C-O-C bond formation.
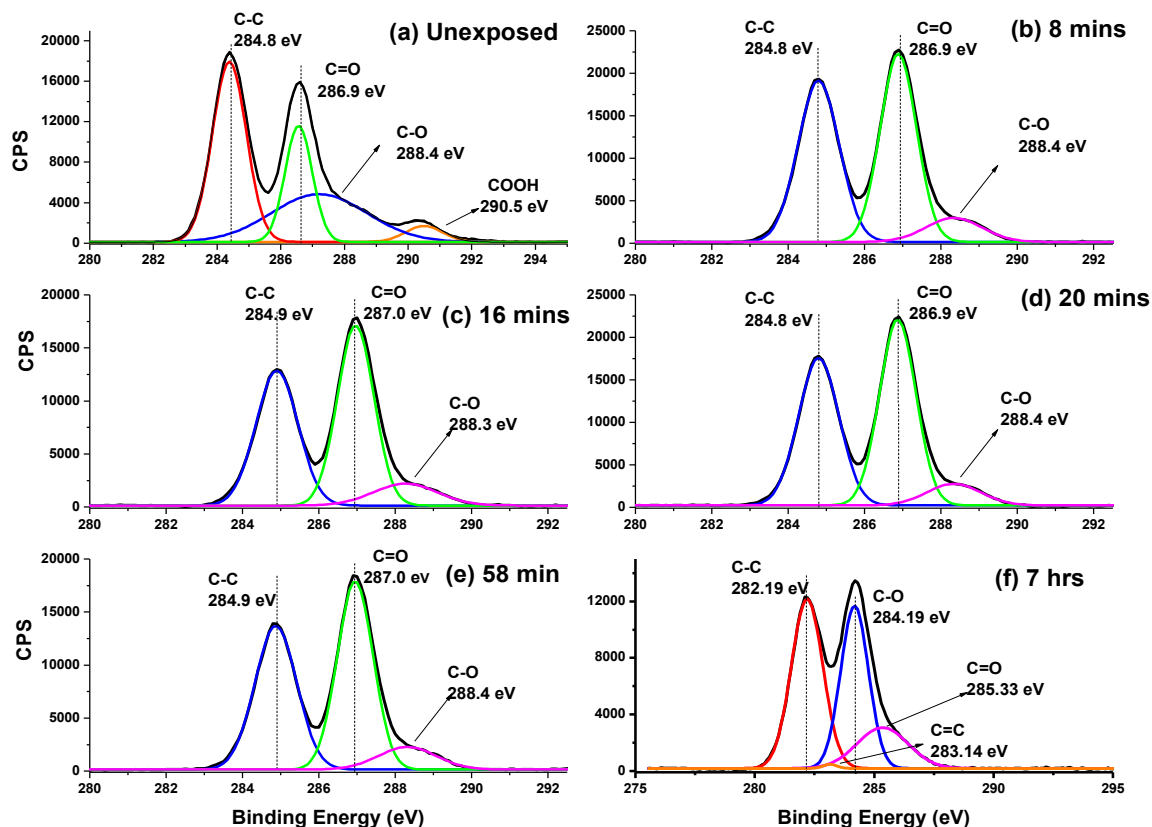
Figure 5-4: The XPS spectrum of unexposed and GOSG exposed for (b) 8min, (c) 16 min, (d) 20 min, (e) 58 min, and (f) 7 hrs

5.3.3 Raman spectroscopy

The recorded Raman spectrum of the unexposed GO thin film and GOSGs thin films are compared in Fig. 5-5. From Fig.5-5a, it is clear that that two main Raman peaks were recorded at wavenumber of 1351 cm^{-1} and 1601 cm^{-1} that are attributed to the D and G bands, respectively [68]. The existence of D band was attributed to the scattering effects between the defects sites and phonons, while the G-band was observed due to the planar configuration of sp^{2} bonded carbon. Two weaker peaks were also recorded at wavenumber of 2697 cm^{-1} and 2930 cm^{-1} that are attributed to the 2D and D+G bands respectively. However for the GOSG samples, the G-band was shifted towards larger wavenumber with shorter treatment time, indicating an increase in the thickness of graphene [82]. The thickness increasing could be

due to the aggregation of the graphene oxide flakes to form the sol-gel structure. The 2D band, which commonly appear due to the presence of graphene structure, was also recorded at wavenumber of 2690 cm^{-1} for both unexposed GO solution and 7 hrs GOSG. Whilst, the 2D band feature in the 8 min, 16 min, 20 min and 58 min GOSGs was recorded at low intensity.

The quality of the graphene layer is generally assessed by means of calculating the I_D/I_G ratio also known as the defect ratio [31]. It was found that the defect ratio increased from 0.85 to 1.26 by reducing the exposure time from 7 hrs to 0. The increase in defect ratio was generally attributed to producing more dislocation sites in the carbon atoms in the aromatic plane [83]. However, it could also be due to introduction of oxygen functional groups into the basal plane of the graphene oxide sheets as well as introduction of hole doping. This could be confirmed from the XPS analysis where it was shown that the intensity of the C-O bond was significantly larger than that of the unexposed.
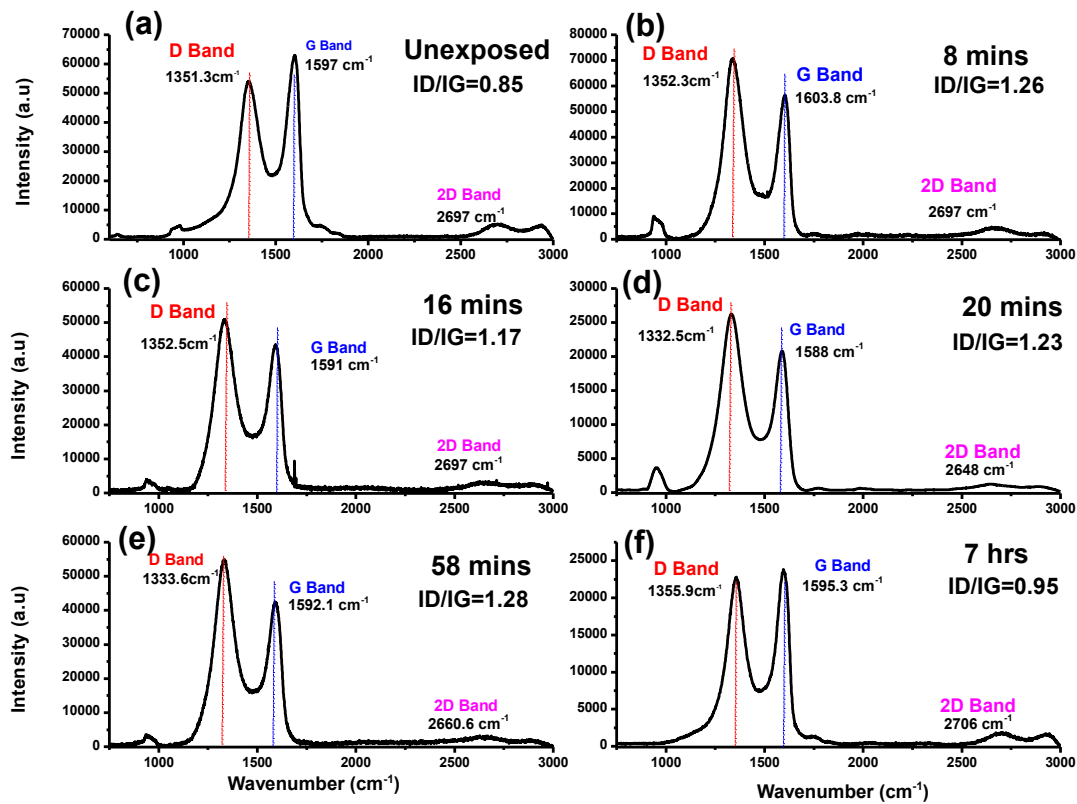
Figure 5-5: The recorded Raman spectrum of (a) unexposed GO and (b) 8 min, (c) 16 min, (d) 20 min, (e) 58 min and (f) 7 hrs laser treated GOSG.

5.3.4 Surface Morphology

Fig.5-6 shows the AFM images of unexposed GO thin films and GOSG thin film fabricated at different exposure time. The average roughness of the deposited thin films of the unexposed GO and GOSGs are compared in Table 5-1. It was found that the highest average roughness were observed in the GOSG with shortest exposure time (i.e. 8 min) and high laser pulse energy (i.e.2 mJ) and larger focal length (i.e.10 cm) as it is evident in Table 5-1. This high roughness could be attributed to the high level of impurities, due to the insufficient exposure time for reducing the GO solution and consequently lack of removal of the OH⁻ components. It was found that the 8 min, 16 min, 20 min and 58 min GOSG possessed the highest average roughness, indicating an irregularity in the stacking of the graphene sheets relative to the

unexposed GO and 7 hrs GOSG. It was found that the 7 hour GOSG offer the smoothest surface with an average roughness of 5.587 nm as shown in Fig.5-6f.
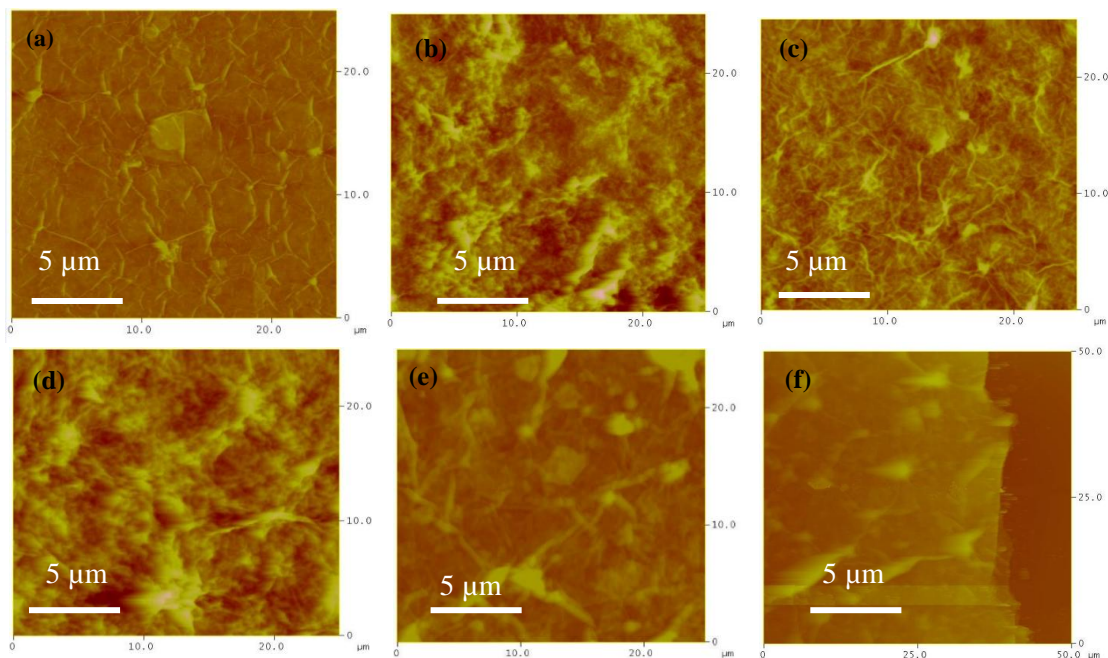
Figure 5-6: The AFM images of (a) unexposed GO, (b) 8 min, (c) 16 min, (d) 20 min, (e) 58 min and (f) 7 hrs GOSG.

Exposure Time	Average Roughness (nm)
Unexposed	11.992
8 min	54.809
16 min	22.57
20 min	29.171
58 min	44.63
7 hrs	5.587

Table 5-1: The average roughness of the GOSG after treatment for various times

The SEM images of GOSG are shown in the Fig.5-7. The SEM images confirm that the smoothest surface was achieved in the GOSG after 7 hrs laser treatment. As can be seen from this figure the wrinkled layers is a common feature in the produced GOSGs by exposing the GO solutions for 8 min, 16 min, 20 min and 58 min. However, the wrinkles, folding and porous structured features were increased as a result of

reducing the exposure time, which is due to the shortage of laser-material interaction time to reduce the oxygen functionalities decorating the graphene oxide flakes. This consequently caused the stacked graphene oxide flakes to become more coarse and thicker than that of 7 hrs GOSG where the film surface
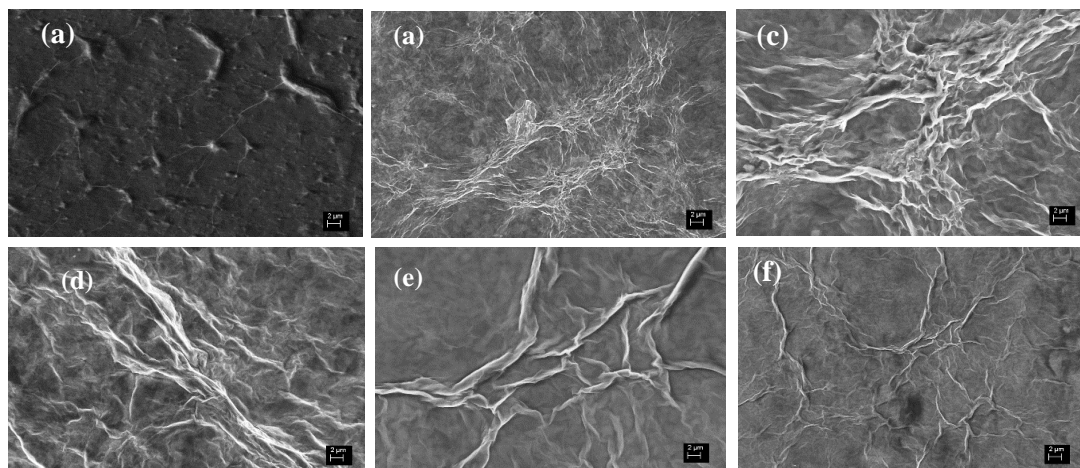
was much smoother.

Figure 5-7: The SEM images of (a) unexposed GO thin film and GOSG thin film exposed for (b) 8 min, (c) 16 min, (d) 20 min, (e) 58 min and (f) 7 hrs.

A further investigation was specifically drawn for the 7 hrs GOSG structure. Fig.5-8 shows the TEM and SEM images of the 7 hrs GOSG. As can be seen from Fig.5-8b inset, it is clear that the GOSG were formed by stacking the GO layers, which was due to the weaker electrostatic interactions and stronger van der Waal forces between the smooth graphene oxide sheets due to lack of hydrogen covalent bond
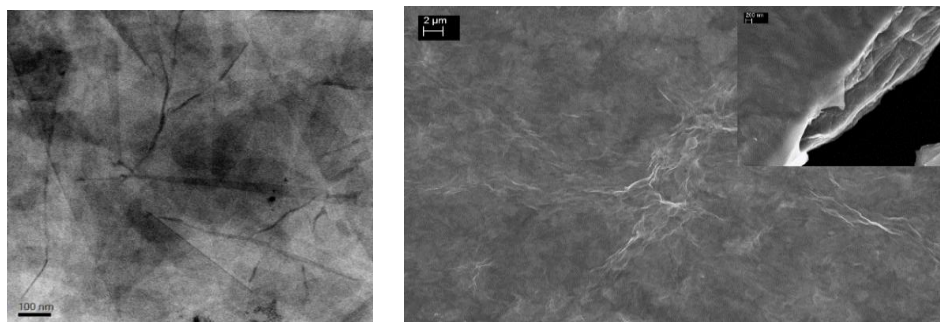
between separated sheets in the GO solution [13].

Figure 5-8: The (a) TEM (b) SEM images of the 7 hrs GOSG. Inset shows the layered structure of the film.

5.3.5 X-ray diffraction

X-Ray diffraction analysis was utilized to study the structural properties of the GOSG films. Lattice planes of (001) and (002) caused diffraction peaks at 11.6° and 23.4° respectively in the unexposed GO film as shown in Fig.5-9 [84]. From this figure, it is clear that a strong and sharp peak which is signature of the presence of carbon atoms in conjunction with oxygen.

It was also found that the peak at 11.6° in the GOSG offers a red shift with decreases in the peak intensity which was attributed to the effects of the laser processing and producing the rGO. This could be attributed to π- π stacking effect between the graphene sheets as a result of the recovery of the carbon bonds after the reduction process and hence the formation of sol-gel structure [81]. Another broad peak centered at approximately 21° was recorded which was assigned to the random packing of graphene oxide sheets [81].
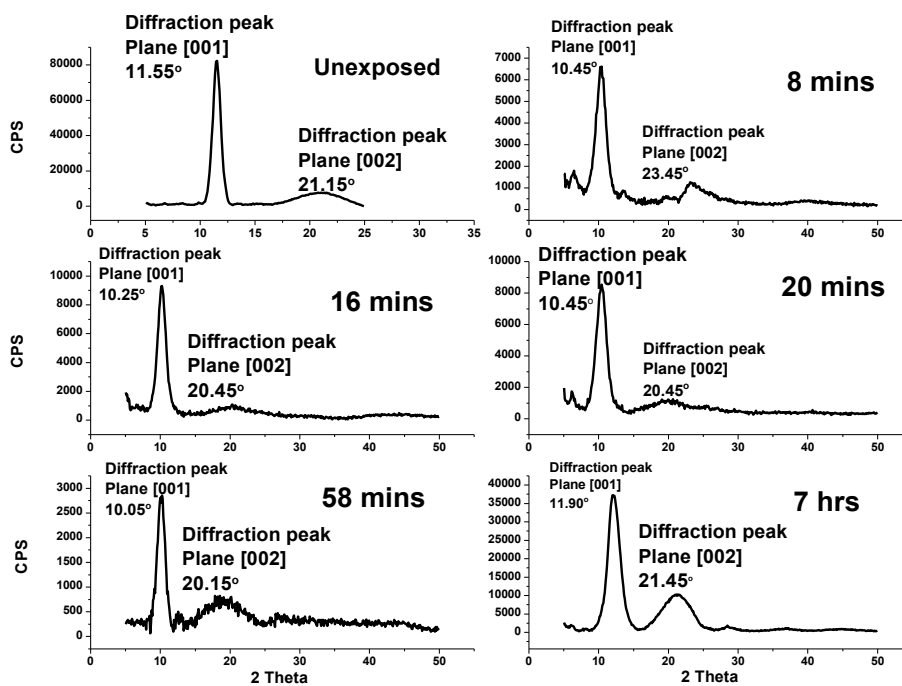
Figure 5-9: The XRD pattern of unexposed GO and the GOSG film.

Using Braggs law the interlayer spacing was calculated. It was found that the interlayer spacing unexposed graphene oxide and 7 hrs GOSG exhibited the smallest interlayer spacing values of 7.52 A$^{\circ}$ and 7.31 A$^{\circ}$ respectively, which coincides with having the smallest defect ratio and intermediate value for the surface morphology. The two larger interlayer spacing values of 8.60 A$^{\circ}$ and 8.86 A$^{\circ}$ were calculated for 8 min and 58 min GOSG films respectively that also corresponds to the two highest values of surface roughness and Raman defect ratio. The XPS analysis showed that all the GOSG obtained at exposure time less than 58 min recorded significantly larger intensities of the C-O bond in comparison to both unexposed and 7 hrs GOSG. This is due to the C=C bond dissociation because of the energetic laser pulses and chemisorption of oxygen functional groups between the graphene oxide sheets, and hence increasing the interlayer spacing. The 16 min and 20 min GOSG indicate interlayer spacing values of 8.57 A$^{\circ}$ and 8.55 A$^{\circ}$ respectively as summarized in the table 5-2.

Table 5-2: The interlayer spacing of the unexposed and GOSG samples.

Exposure Time	d (A°)
Unexposed	7.52
8 min	8.60
16 min	8.57
20 min	8.55
58 min	8.86
7 hrs	7.31

5.4 Summary

This chapter discussed and analyzed a novel graphene oxide sol-gel fabrication process. The method of fabrication largely depends on the position of laser focal point on the GO solution-air interface. After manipulating the GO solution volume, laser intensity and focal length, it was found that the GOSG could be formed 8 min, 16 min, 20 min, 58 min and 7 hrs.

FTIR spectroscopy shows that the 7 hrs GOSG pertained to a behaviour similar to graphene with the highest transmission compared to the other GOSGs. The sp^2 hybridized C=C bonds were found to be dissociated as a result of the high intensity laser pulses and consequently the absorbance of the C=C transition was decreased as shown in Fig.5-3. The introduction of oxygen atoms into the graphene oxide sheets via chemisorption was also found as recording the C=O transition which was also confirmed by the Raman spectroscopy. From surface morphology analysis, using AFM and SEM it was found that all the GOSG thin films except the 7 hrs one provided high surface roughness and porous surface area with

randomly stacked graphene oxide layers. The smooth layered stacking structure and the smallest average surface roughness was obtained in the 7 hrs GOSG. XPS analysis shown that the amount of the COOH was reduced by disappearing the COOH peak in all GOSGs spectra. The interlayer distance between the graphene oxide sheets was increased by increasing the exposure time from 8 min to 58 min was calculated in the range of 8.55 A^{o} to-8.86 A^{o} relative to the unexposed 7.52 A^{o}. However the 7 hrs GOSG showed the smallest interlayer distance of 7.31 A^{o}.

Chapter 6

Conclusions and future work

_____

6.1 Summary

6.2 Future work

_____

6.1 Summary

A branch of the revolution in the study of graphene since 2004 is graphene oxide and how it is used and fabricated. In this study, successful reduction of graphene oxide aqueous solution was carried out by means of using ultrafast laser interaction with the GO aqueous solution using different techniques. It was found that using ultrashort duration laser pulses produces thinner and smoother GO flakes with enhanced electrical properties relative to GO treated with UV light and other photo treated techniques [30].

Fs laser pulses of laser energy of 250 μJ and wavelength of 800 nm were initially used for reducing the GO aqueous solutions at two different concentrations of 0.5 mg/ml and 6.2 mg/ml. By adjusting the laser focal point a few of millimeter under the surface, the average mean roughness of the GO flakes was reduced by 66% and 95.6% respectively for rGO1 and rGO2 thin films after 6 hrs exposure. The I_D/I_G ratio of rGO1 and rGO2 were also reduced by 7% and 6% respectively after 6 hrs laser treatment. It was also shown that using higher concentration of GO solution enhanced the resistivity of rGO films by reducing its value by 4 orders of magnitude which could raise the electron mobility of the rGO films close to that of pristine graphene films.

The XPS analysis showed that after laser treatment the C/O atomic ratio of both rGO1 and rGO2 films increases by 1.10x and 3x respectively. It was also shown that the FWHM ratio of the C1s and O1s of the rGO2 solution was increased by a factor of 1.55 whereas no significant changes were observed in the GO1 solution. Hence, it can be concluded that fs laser treatment can invariably enhance the material and physical properties of high concentration graphene oxide relative to that of low concentration.

This study has also uncovered a vastly rapid method to produce GOSG as less as 8 mins in comparison to the GO gel obtained by chemical and thermal treatments discussed in Chapter 2, which nevertheless required many hours to obtain. Sol-gel graphene oxide can be used in numerous applications such as conductive ink and as semi-conducting layer in nano devices.

By placing the laser focal point at the air/GO aqueous solution interface and manipulating the laser energy, ablated volume and focal length, the GOSG was acquired after different times in the range of 8 mins to 7 hrs. From the chemical analysis, it was shown that the exposure process resulted in the removal of the OH and water molecules accompanied with dissociation of the sp^2 bonds and chemisorption of oxygen atoms/oxygen functional groups into the basal plane of the graphene oxide sheets. From surface morphology study it was shown that large surface roughness, warping and complex structures was observed in the GOSGs were exposed in the range of 8 min to 58 min whilst the 7 hrs GOSG offered smoother layered graphene-like structure. The defect ratio was increased in the GOSG relative to the unexposed GO aqueous solution, suggesting the increase of hole doping and introduction of oxygen functional groups into the graphene oxide plane, such as the C-O-C bond which acts as a cross linker between the graphene oxide sheets.

6.2 Future work

The usage of wide range of laser energy rather than the 250 μJ to achieve the GO thin film with lowest defect ratio. As it was shown in Chapter 4, oxygen was introduced into the basal plane of the GO sheets via chemisorption as a result of the laser treatment, therefore application of lower/higher energy laser pulses it is essential for optimizing laser treatment parameter to achieve the rGO solution with larger conductivity and higher transmittance close to the pristine graphene.

The GOSG samples were fabricated using a novel fabrication technique, therefore this study has plenty of room for development. The electrical and physical properties of the fabricated GOSG can be improved by more laser parameter optimization and GO concentration. For example, GOSG conductivity is one of the most important factors that needs to be optimized, which depends on the amount of OH in the GOSG solution. The OH concentration can be minimized by increasing the exposure time beyond the point of

yielding the honey-like texture, aiming to reach a complete vaporization of the water content. In addition, the GOSG quality can be enhanced by post exposure after GOSG fabrication. Therefore a GOSG quality can be improved by using a magnetic stirrer during the irradiation process that keep the GO solution more homogenous during the laser treatment to avoid the GO sheets agglomeration and floating on the solution surface, and therefore ensuring that the laser is interacting with a homogenous material at all times.

References

1. Wolf, E.L., *Graphene; A new paradigm in condensed matter and device physics*. 1 ed, ed. Oxford. 2014, United Kingdom: Oxford: University Press. 303.
2. Novoselov, K.S., et al., *Electric Field Effect in Atomically Thin Carbon Films.* Science, 2004. **306**(5696): p. 666-669.
3. Geim, A.K., *Graphene: Status and Prospects.* Science, 2009. **324**(5934): p. 1530-1534.
4. Geim, A.K. and K.S. Novoselov, *The rise of graphene.* Nat Mater, 2007. **6**(3): p. 183-191.
5. Tombros, N., et al., *Electronic spin transport and spin precession in single graphene layers at room temperature.* Nature, 2007. **448**(7153): p. 571-574.
6. Blake, P., et al., *Making graphene visible.* Applied Physics Letters, 2007. **91**(6): p. 063124.
7. Hollister, S.J., *Porous scaffold design for tissue engineering.* Nat Mater, 2005. **4**(7): p. 518-524.
8. Holzinger, M., A. Le Goff, and S. Cosnier, *Nanomaterials for biosensing applications: a review.* Frontiers in Chemistry, 2014. **2**: p. 63.
9. Schwierz, F., *Graphene transistors.* Nat Nano, 2010. **5**(7): p. 487-496.
10. A. H. Castro Neto, F.G., and N. M. R. Peres, *Drawing conclusions from graphene.* Physics World 2006. **33**(19).
11. Sutter, P., *Epitaxial graphene: How silicon leaves the scene.* Nat Mater, 2009. **8**(3): p. 171-172.
12. Strudwick, A.J., et al., *Chemical Vapor Deposition of High Quality Graphene Films from Carbon Dioxide Atmospheres.* ACS Nano, 2015. **9**(1): p. 31-42.
13. Rao, C.N.R., U. Maitra, and H.S.S.R. Matte, *Synthesis, Characterization, and Selected Properties of Graphene*, in *Graphene*. 2012, Wiley-VCH Verlag GmbH & Co. KGaA. p. 1-47.
14. Park, L.-Y.M.a.S.-J., *Preparation and Characterization of Reduced Graphene Nanosheets via Pre-exfoliation of Graphite Flakes.* Bulletin of the Korean Chemical Society, 2012. **33**(1): p. 209-214.
15. Kim, J.H., et al., *Large-Scale Plasma Patterning of Transparent Graphene Electrode on Flexible Substrates.* Langmuir, 2015. **31**(9): p. 2914-2921.
16. Sur, U.K., *Graphene: A Rising Star on the Horizon of Materials Science.* International Journal of Electrochemistry, 2012. **2012**: p. 12.
17. Mayorov, A.S., et al., *Micrometer-Scale Ballistic Transport in Encapsulated Graphene at Room Temperature.* Nano Letters, 2011. **11**(6): p. 2396-2399.
18. Andronico, M. *5 Reasons Graphene Will Change Gadgets Forever*. 2014 [cited 2015 12 July]; Available from: http://blog.laptopmag.com/graphene-tech-uses.
19. Z, E. *Why are Pi bonds weaker than Sigma bonds?* 2014 [cited 2015 28 July]; Available from: http://socratic.org/questions/why-are-pi-bonds-weaker-than-sigma-bonds.
20. Hummers, W.S. and R.E. Offeman, *Preparation of Graphitic Oxide.* Journal of the American Chemical Society, 1958. **80**(6): p. 1339-1339.
21. Chen, J., et al., *An improved Hummers method for eco-friendly synthesis of graphene oxide.* Carbon, 2013. **64**(0): p. 225-229.
22. Bai, H., et al., *On the Gelation of Graphene Oxide.* The Journal of Physical Chemistry C, 2011. **115**(13): p. 5545-5551.
23. Guo, C.X., et al., *Biointerface by Cell Growth on Layered Graphene–Artificial Peroxidase–Protein Nanostructure for In Situ Quantitative Molecular Detection.* Advanced Materials, 2010. **22**(45): p. 5164-5167.
24. Wang, D.-W., et al., *3D Aperiodic Hierarchical Porous Graphitic Carbon Material for High-Rate Electrochemical Capacitive Energy Storage.* Angewandte Chemie International Edition, 2009. **48**(9): p. 1525-1525.
25. Gupta, P., K. Vermani, and S. Garg, *Hydrogels: from controlled release to pH-responsive drug delivery.* Drug Discovery Today, 2002. **7**(10): p. 569-579.
26. Burress, J.W., et al., *Graphene Oxide Framework Materials: Theoretical Predictions and Experimental Results.* Angewandte Chemie International Edition, 2010. **49**(47): p. 8902-8904.

27. Xu, Y., et al., *Self-Assembled Graphene Hydrogel via a One-Step Hydrothermal Process.* ACS Nano, 2010. **4**(7): p. 4324-4330.

28. Paton, K.R., et al., *Scalable production of large quantities of defect-free few-layer graphene by shear exfoliation in liquids.* Nat Mater, 2014. **13**(6): p. 624-630.

29. Park, G.D., et al., *Large-Scale Production of MoO3-Reduced Graphene Oxide Powders with Superior Lithium Storage Properties by Spray-Drying Process.* Electrochimica Acta, 2015. **173**: p. 581-587.

30. KUMAR, P., K.S. SUBRAHMANYAM, and C.N.R. RAO, *GRAPHENE PRODUCED BY RADIATION-INDUCED REDUCTION OF GRAPHENE OXIDE.* International Journal of Nanoscience, 2011. **10**(04n05): p. 559-566.

31. Trusovas, R., et al., *Reduction of graphite oxide to graphene with laser irradiation.* Carbon, 2013. **52**(0): p. 574-582.

32. Chang, H.-W., et al., *Reduction of graphene oxide in aqueous solution by femtosecond laser and its effect on electroanalysis.* Electrochemistry Communications, 2012. **23**(0): p. 37-40.

33. Ledoux, G., et al., *Facile and rapid synthesis of highly luminescent nanoparticles via pulsed laser ablation in liquid.* Nanotechnology, 2009. **20**(44): p. 445605.

34. Huang, L., et al., *Pulsed laser assisted reduction of graphene oxide.* Carbon, 2011. **49**(7): p. 2431-2436.

35. Pan, D., et al., *Li Storage Properties of Disordered Graphene Nanosheets.* Chemistry of Materials, 2009. **21**(14): p. 3136-3142.

36. Gengler, R.Y.N., et al., *Revealing the ultrafast process behind the photoreduction of graphene oxide.* Nat Commun, 2013. **4**.

37. Kymakis, E., et al., *Laser-Assisted Reduction of Graphene Oxide for Flexible, Large-Area Optoelectronics.* Selected Topics in Quantum Electronics, IEEE Journal of, 2014. **20**(1): p. 106-115.

38. Spanò, S., et al., *Tunable properties of graphene oxide reduced by laser irradiation.* Applied Physics A, 2014. **117**(1): p. 19-23.

39. Shang, J., et al., *The Origin of Fluorescence from Graphene Oxide.* Scientific Reports, 2012. **2**: p. 792.

40. Zhou, S. and A. Bongiorno, *Origin of the Chemical and Kinetic Stability of Graphene Oxide.* Scientific Reports, 2013. **3**: p. 2484.

41. Jang, J., et al., *Effects of the alkylamine functionalization of graphene oxide on the properties of polystyrene nanocomposites.* Nanoscale Research Letters, 2014. **9**(1): p. 265-265.

42. Nethravathi, C. and M. Rajamathi, *Chemically modified graphene sheets produced by the solvothermal reduction of colloidal dispersions of graphite oxide.* Carbon, 2008. **46**(14): p. 1994-1998.

43. Dreyer, D.R., et al., *The chemistry of graphene oxide.* Chemical Society Reviews, 2010. **39**(1): p. 228-240.

44. Wu, T., et al., *Production of Reduced Graphene Oxide by UV Irradiation.* Journal of Nanoscience and Nanotechnology, 2011. **11**(11): p. 10078-10081.

45. Guardia, L., et al., *UV light exposure of aqueous graphene oxide suspensions to promote their direct reduction, formation of graphene–metal nanoparticle hybrids and dye degradation.* Carbon, 2012. **50**(3): p. 1014-1024.

46. Ding, Y.H., et al., *A green approach to the synthesis of reduced graphene oxide nanosheets under UV irradiation.* Nanotechnology, 2011. **22**(21): p. 215601.

47. Kim, S.R., M.K. Parvez, and M. Chhowalla, *UV-reduction of graphene oxide and its application as an interfacial layer to reduce the back-transport reactions in dye-sensitized solar cells.* Chemical Physics Letters, 2009. **483**(1–3): p. 124-127.

48. Solís-Fernández, P., et al., *Determining the thickness of chemically modified graphenes by scanning probe microscopy.* Carbon, 2010. **48**(9): p. 2657-2660.

49.   Paredes, J.I., et al., *Atomic Force and Scanning Tunneling Microscopy Imaging of Graphene Nanosheets Derived from Graphite Oxide.* Langmuir, 2009. **25**(10): p. 5957-5968.

50.   Mungse, H.P. and O.P. Khatri, *Chemically Functionalized Reduced Graphene Oxide as a Novel Material for Reduction of Friction and Wear.* The Journal of Physical Chemistry C, 2014. **118**(26): p. 14394-14402.

51.   Mattevi, C., et al., *Evolution of Electrical, Chemical, and Structural Properties of Transparent and Conducting Chemically Derived Graphene Thin Films.* Advanced Functional Materials, 2009. **19**(16): p. 2577-2583.

52.   Rück-Braun, K., et al., *Formation of Carboxy- and Amide-Terminated Alkyl Monolayers on Silicon(111) Investigated by ATR-FTIR, XPS, and X-ray Scattering: Construction of Photoswitchable Surfaces.* Langmuir, 2013. **29**(37): p. 11758-11769.

53.   Some, S., et al., *High-Quality Reduced Graphene Oxide by a Dual-Function Chemical Reduction and Healing Process.* Sci. Rep., 2013. **3**.

54.   Zhang, M., et al., *Production of Graphene Sheets by Direct Dispersion with Aromatic Healing Agents.* Small, 2010. **6**(10): p. 1100-1107.

55.   Xu, Y., et al., *Three-dimensional self-assembly of graphene oxide and DNA into multifunctional hydrogels.* ACS Nano, 2010. **4**(12): p. 7358-62.

56.   Ai, W., et al., *Formation of graphene oxide gel via the [small pi]-stacked supramolecular self-assembly.* RSC Advances, 2012. **2**(32): p. 12204-12209.

57.   Alt, H.G., et al., *Metallacyclic metallocene complexes as catalysts for olefin polymerization.* Coordination Chemistry Reviews, 2006. **250**(1–2): p. 2-17.

58.   Kandidov, V.P., et al., *Self-transformation of a powerful femtosecond laser pulse into a white-light laser pulse in bulk optical media (or supercontinuum generation).* Applied Physics B, 2003. **77**(2-3): p. 149-165.

59.   Sato, Y., et al., *Synthesis of polyyne molecules from hexane by irradiation of intense femtosecond laser pulses.* Carbon, 2010. **48**(5): p. 1673-1676.

60.   Chen, J., et al., *Controllable fabrication of ultrathin free-standing graphene films.* Philosophical Transactions of the Royal Society of London A: Mathematical, Physical and Engineering Sciences, 2014. **372**(2013).

61.   Li, Z., et al., *Quantitative determination of the spatial orientation of graphene by polarized Raman spectroscopy.* Carbon, 2015. **88**(0): p. 215-224.

62.   Thema, F.T., et al., *Synthesis and Characterization of Graphene Thin Films by Chemical Reduction of Exfoliated and Intercalated Graphite Oxide.* Journal of Chemistry, 2013. **2013**: p. 6.

63.   Cheng, S.F., et al., *Selective area metalorganic vapor-phase epitaxy of gallium arsenide on silicon.* Journal of Crystal Growth, 2008. **310**(3): p. 562-569.

64.   Chiang, T.C. and F. Seitz, *Photoemission spectroscopy in solids.* Annalen der Physik, 2001. **10**(1-2): p. 61-74.

65.   Yumitori, S., *Correlation of C1s chemical state intensities with the O1s intensity in the XPS analysis of anodically oxidized glass-like carbon samples.* Journal of Materials Science, 2000. **35**(1): p. 139-146.

66.   Meng, L.-Y. and J. Park, *Preparation and Characterization of Reduced Graphene Nanosheets via Pre-exfoliation of Graphite Flakes.* Bull. Korean Chem. Soc., 2012. **33**(1): p. 209.

67.   Yang, D., et al., *Chemical analysis of graphene oxide films after heat and chemical treatments by X-ray photoelectron and Micro-Raman spectroscopy.* Carbon, 2009. **47**(1): p. 145-152.

68.   Ferrari, A.C., *Raman spectroscopy of graphene and graphite: Disorder, electron–phonon coupling, doping and nonadiabatic effects.* Solid State Communications, 2007. **143**(1–2): p. 47-57.

69.   Rani, J.R., et al., *Epoxy to Carbonyl Group Conversion in Graphene Oxide Thin Films: Effect on Structural and Luminescent Characteristics.* The Journal of Physical Chemistry C, 2012. **116**(35): p. 19010-19017.

70. Saito, R., et al., *Raman spectroscopy of graphene and carbon nanotubes.* Advances in Physics, 2011. **60**(3): p. 413-550.

71. Saito, R., et al., *Probing Phonon Dispersion Relations of Graphite by Double Resonance Raman Scattering.* Physical Review Letters, 2001. **88**(2): p. 027401.

72. Boström, M. and B.E. Sernelius, *Repulsive van der Waals forces due to hydrogen exposure on bilayer graphene.* Physical Review A, 2012. **85**(1): p. 012508.

73. Chua, C.K., A. Ambrosi, and M. Pumera, *Graphene oxide reduction by standard industrial reducing agent: thiourea dioxide.* Journal of Materials Chemistry, 2012. **22**(22): p. 11054-11061.

74. Oh, J., et al., *Graphene oxide porous paper from amine-functionalized poly(glycidyl methacrylate)/graphene oxide core-shell microspheres.* Journal of Materials Chemistry, 2010. **20**(41): p. 9200-9204.

75. Zu, S.-Z. and B.-H. Han, *Aqueous Dispersion of Graphene Sheets Stabilized by Pluronic Copolymers: Formation of Supramolecular Hydrogel.* The Journal of Physical Chemistry C, 2009. **113**(31): p. 13651-13657.

76. Akhavan, O., *The effect of heat treatment on formation of graphene thin films from graphene oxide nanosheets.* Carbon, 2010. **48**(2): p. 509-519.

77. Pei, S. and H.-M. Cheng, *The reduction of graphene oxide.* Carbon, 2012. **50**(9): p. 3210-3228.

78. Banks, R.C. *Bonding and Hybridization* May 2002 [cited 2015 28 July]; Available from: https://chemistry.boisestate.edu/richardbanks/inorganic/bonding%20and%20hybridization/bonding_hybridization.htm.

79. Kong, X.-k., Q.-w. Chen, and Z.-y. Lun, *Probing the influence of different oxygenated groups on graphene oxide's catalytic performance.* Journal of Materials Chemistry A, 2014. **2**(3): p. 610-613.

80. Zhang, H., D. Hines, and D.L. Akins, *Synthesis of a nanocomposite composed of reduced graphene oxide and gold nanoparticles.* Dalton Transactions, 2014. **43**(6): p. 2670-2675.

81. Wu, Y., et al., *Graphene/liquid crystal based terahertz phase shifters.* Optics Express, 2013. **21**(18): p. 21395-21402.

82. Changjing Fu*, G.Z., Haijun Zhang, Shuang Li, *Evaluation and Characterization of Reduced Graphene Oxide Nanosheets as Anode Materials for Lithium-Ion Batteries.* International Journal of Electrochemical science, 2013. **8**: p. 12.

83. Joe Hodkiewicz, *Characterizing Graphene with Raman Spectroscopy*, T.F. Scientific, Editor. 2010: Madison, WI, USA.

84. Butz, B., et al., *Dislocations in bilayer graphene.* Nature, 2014. **505**(7484): p. 533-537.

85. Xiong, Z., et al., *Photocatalytic degradation of dyes over graphene-gold nanocomposites under visible light irradiation.* Chemical Communications, 2010. **46**(33): p. 6099-6101.